Biol Cybern (2016) 110:359–382
DOI 10.1007/s00422-016-0696-4

REVIEW

Biological
Cybernetics

Internally coupled ears: mathematical structures and mechanisms underlying ICE

Anupam P. Vedurmudi[1] · **Bruce A. Young**[2] · **J. Leo van Hemmen**[1]

Received: 6 June 2016 / Accepted: 13 September 2016 / Published online: 25 October 2016

Abstract In internally coupled ears (ICE), the displacement of one eardrum creates pressure waves that propagate through air-filled passages in the skull, causing a displacement of the opposing eardrum and vice versa. In this review, a thorough mathematical analysis of the membranes, passages, and propagating pressure waves reveals how internally coupled ears generate unique amplitude and temporal cues for sound localization. The magnitudes of both of these cues are directionally dependent. On the basis of the geometry of the interaural cavity and the elastic properties of the two eardrums confining it at both ends, the present paper reviews the mathematical theory underlying hearing through ICE and derives analytical expressions for eardrum vibrations as well as the pressures inside the internal passages, which ultimately lead to the emergence of highly directional hearing cues. The derived expressions enable one to explicitly see the influence of different parts of the system, e.g., the interaural cavity and the eardrum, on the internal coupling, and the frequency dependence of the coupling. The tympanic fundamental frequency segregates a low-frequency regime with constant time-difference magnification (time dilation factor) from a high-frequency domain with considerable amplitude magnification. By exploiting the physical properties of the coupling, we describe a concrete method to numerically estimate the eardrum's fundamental frequency and damping solely through measurements taken from a live animal.

Keywords Internally coupled ears · Bioacoustics · Acoustic coupling · Sound localization · Tympanic vibrations · Fundamental frequency

1 Introduction

Internally coupled ears, or ICE, is a terrestrial vertebrate hearing system in which the two tympanic membranes (eardrums) are functionally coupled by anatomical connections through the skull. It occurs in most frogs, lizards, alligators, and birds; conservatively, it is estimated to be more than 15,000 species or roughly half of the terrestrial vertebrates. In ICE, the eardrums are driven by a combination of external sound pressure and internal cavity pressure resulting from the coupled vibration of the opposite eardrums (Autrum 1942; Christensen-Dalsgaard and Manley 2005; Vossen et al. 2010); cf. Fig. 1b, c. If the distance L between the eardrums (the interaural distance) is small, the time difference between excitation of the opposing membranes due to an external pressure is too small for effective neuronal processing, precluding sound localization through temporal cues. Furthermore, for many ICE animals, the interaural level (or intensity) difference (ILD) is negligible, irrespectively of the source direction. With ICE, however, an animal can amplify the time differences as well as generate considerable (e.g., about 20 dB) direction-dependent amplitude differences between the eardrum vibrations. Thus, ICE enables even animals with small interaural distance, say a few cm, to localize sound.

This article belongs to a Special Issue on Internally Coupled Ears (ICE).

✉ J. Leo van Hemmen
lvh@tum.de

Anupam P. Vedurmudi
anupam.vedurmudi@tum.de

Bruce A. Young
byoung@atsu.edu

[1] Physik Department T35 and BCCN–Munich, Technische Universität München, 85747 Garching bei München, Germany

[2] Kirksville College of Osteopathic Medicine, A.T. Still University, Kirksville, MO 63501, USA

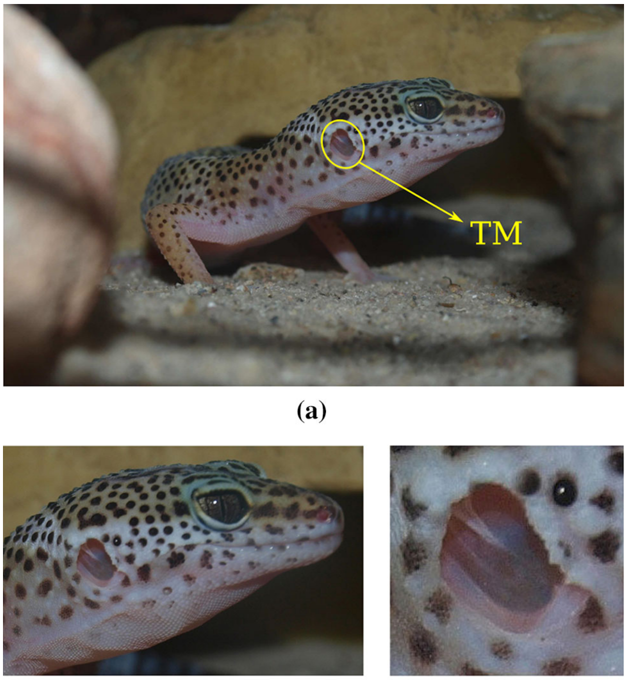

(a)

(b)

(c)

Fig. 1 *Top* Leopard gecko—a typical animal with ICE. The location of the eardrum or tympanic membrane (TM) on the side of its head has been highlighted. *Bottom left* Close-up of its head, where its eardrum as well as the embedded extracolumella (brighter protrusion, *top-left*), can be discerned clearly. The vibrations of one the eardrums excite the air inside the cavity, which in turn influences the vibrations of the opposite eardrum and vice versa. *Bottom right* Close-up of the eardrum. The lighter-colored protrusion on the top-left of the tympanum is the extracolumella, which transfers the eardrum vibrations, via the columella, to the cochlea; cf. Figs. 3b and 6a, b. Photograph courtesy of Prof. Frieder Mugele (University of Twente). **a** Leopard gecko, **b** close-up of the Leopard gecko's head, **c** close-up of the eardrum

Whether and how it does so neuronally is not a focus of the present paper, aside from a few remarks in the discussion (Sect. 5).

An earlier analytical paper (Vossen et al. 2010) was formulated to explain a set of experimental data gathered from a few selected species of Gekkonid lizards (Christensen-Dalsgaard and Manley 2005). More recently, we have presented a general model of ICE (Vedurmudi et al. 2016) intended to be applicable to all ICE animals. The format of the work presented by Vedurmudi et al. (2016) precluded a full presentation of not only the mathematical arguments, but also some of the interesting, and biologically relevant, issues that arise from a consideration of ICE. The present contribution presents a review of the full model, an expansion into topics not covered by Vedurmudi et al. (2016), and a more detailed derivation of some of the fundamental concepts.

There is a substantial difference between the mathematical modeling presented in the present Review, based on only two predecessors (Vossen et al. 2010; Vedurmudi et al. 2016), and the older literature that is comprehensively described by Fletcher (1992) and also running under the name of "pressure-gradient receiver." As shown elsewhere (van Hemmen et al. 2016), this name is definitely *not* what ICE boils down to. Actually, it is just the opposite since the ensuing differences are not infinitesimal, which one would need for taking a gradient, but as large as possible. Whereas the latter theory is linear-response theory with impedances as fit parameters, the present ICE analysis is based on the mere geometry of the interaural cavity and can do without any fit parameter.

Previous experimental work (Manley 2000) has shown that lizards have two distinct populations of cochlear hair cells—one that responds to amplitude cues and the other to temporal cues. Ultimately, these two hair-cell populations both project bilaterally, giving the organism a neuronal template to contrast both the amplitude and temporal patterns (Szpir et al. 1990) arising from the tympana. We are following (Jørgensen et al. 1991) in postulating an algorithm for determining amplitude (level) differences. More specifically, we assume that this is done by a neuronal subtraction of logarithmic vibration amplitudes of the two membranes. The biological physics is that of hair-cell response being governed by the (Weber–Fechner) logarithm of the amplitude, whereas the "subtraction" is that of excitation minus inhibition (E/I) and need not be taken literally as it is simply used here as a criterion. We refer to this subtraction as the internal level difference (**i**LD) and contrast it with the interaural level difference (**I**LD), i.e., the logarithmic amplitude difference between the *external* sound inputs to both ears.

It is also known that certain neurons are sensitive to time differences between eardrum vibrations (Schnupp and Carr 2009; Christensen-Dalsgaard et al. 2011; Christensen-Dalsgaard and Carr 2009). We refer to this metric as the internal time difference (iTD), in contrast to the interaural time difference (ITD) as measured by an external observer. The internal time and level differences are the unique outcome of the interaction between the outside signal and the internal coupling arising from the air-filled interaural cavity as shown in see Fig. 2.

The model (Vedurmudi et al. 2016) explained here explicitly demonstrates how iTDs and iLDs emerge solely due to the internal acoustic coupling between the eardrums in conjunction with external left and right stimulus. We do so through a minimal model of circular membranes coupled through a cylindrical air-filled cavity. The model will be "minimal" in the sense that the number of its ingredients is as small as possible and its structure is as simple as possible, but not simpler. Furthermore, and due to its simplicity, we will see that that the present ICE Model is *universal* in the sense that with an appropriate change in parameters, it is applicable to all species with internally coupled ears. Finally, the ultimate goal of the present review is proving that the inter-

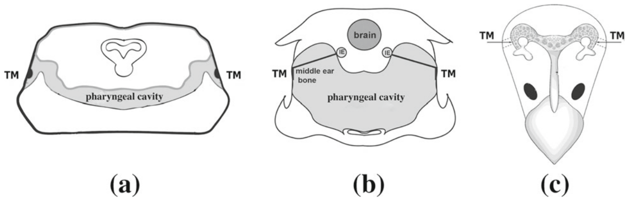

Fig. 2 Interaural cavity connecting *left* and *right* tympanum (TM) in **a** frogs, **b** lizards, and **c** birds. The bird in **c** is seen from the *top*, the other two show a cross section, and all three exhibit the interaural cavity as a gray tube. In **a**, **b** it is part of the pharyngeal cavity (pharynx), in **c** it is a separate tube through the skull. Little bones (extracolumellae) embedded in the eardrums transfer their vibrations to *left* and *right* cochlea. In all three cases, the eardrum (TM) separates the pharyngeal or interaural cavity from the external world. Figure from (Christensen-Dalsgaard 2005), redrawn

play of the geometry and the biophysics of the two tympana, and the cavity connecting them—cf. Fig. 3b—, suffices to qualitatively understand the main properties of ICE.

2 Mathematical ICE model

Our aims are to devise a mathematical model for azimuthal sound localization and, thereafter, to compare it with experimental data. To do so, we must first model the anatomy of animals with ICE. The ICE system and, hence, our model, has three primary components,

- the sound source and the animal's head which gives us a mathematical expression for the stimulus at the eardrums.
- the eardrum itself, which both receive the external stimuli and separate the outside auditory world from the inside pharyngeal cavity connecting the two eardrums. And finally,
- the interaural or pharyngeal cavity, which, with the Eustachian tube, is responsible for the coupling that leads to the modification and often enhancement of the hearing cues.

Once the above biophysical systems have been described, we can proceed with a mathematical analysis of the different components in order to derive explicit expressions for the hearing cues. Though the ICE theory to be explained is universal and far more general, we will focus on lizards for the sake of definiteness.

2.1 Internal cavity

We model the internal cavity as an air-filled cylinder of length L, commonly termed the interaural distance, obtained through direct measurement. Similarly, the cavity volume V_{cav} can be measured directly and can be used to calculate the cylinder radius through the relation

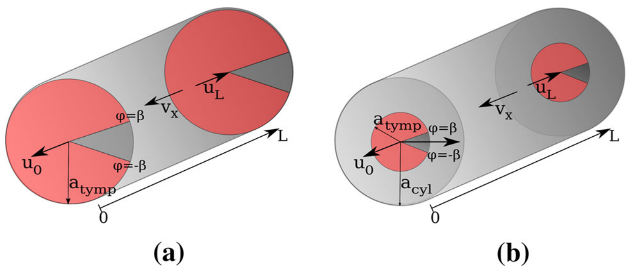

Fig. 3 The *bold arrows* represent the direction conventions along the cylinder's axis. The present model **b** is represented by a cylinder of radius a_{cyl} and length L closed at both ends by sectorial membranes of radius a_{tymp}. The darkly shaded v-shaped region corresponds to the extracolumella; see Sect. 2.2.1. The membranes are driven both by an external sound pressure as well as by the internal pressure inside the cavity (lightly shaded region). The membrane motion in turn moves the extracolumella like a second-order lever, i.e., the load is situated between the effort and the fulcrum. Finally, the extracolumella transduces the membrane vibration via the columella to the cochlea; cf. Fig. 5. **a** Internal cavity—previous model (Vossen et al. 2010) without volume correction. **b** Internal cavity—current model (Vedurmudi et al. 2016) allowing volume correction with $a_{\text{tymp}} < a_{\text{cyl}}$

$$a_{\text{cyl}} = \sqrt{\frac{V_{\text{cav}}}{\pi L}} \tag{1}$$

The three-dimensional model for the internal cavity is illustrated in Fig. 3b. The smaller circles at either end of the cylinder correspond to the eardrums. Simply put, the model consists of a cylindrical tube of radius a_{cyl} and length L with circular holes on either side with the radius of the tympanic membrane, $a_{\text{tymp}} \leq a_{\text{cyl}}$. These holes are in turn closed by rigidly clamped elastic membranes, the tympana (darkly shaded circular surfaces in Fig. 3b), which will be described in the next section.

In an earlier mathematical treatment of ICE (Vossen (2010); Vossen et al. (2010)), the oral cavity was modeled as a simple cylinder closed at both ends by rigidly clamped (baffled) circular eardrums. In the aforementioned model (cf. Fig. 3a), the cylinder length is the interaural distance L, and the radius of the cylinder was taken to be equal to that of the eardrum, i.e., $a_{\text{cyl}} = a_{\text{tymp}}$, which resulted in a cavity volume about an order of magnitude smaller than what is observed in nature. This air-filled cavity is not the mouth or oral cavity but the *pharyngeal* cavity, which is often appreciably smaller. In general, we will see that a smaller volume results in a stronger interaural coupling. By treating the cavity volume as a variable parameter, we can directly analyze its effect on the internal coupling between the two eardrums, and the effect this has on the iTD and iLD. In doing so we will meet several new and surprising phenomena, and the great reward of a universal theory is that it provides general insight.

The exact nature of the internal coupling will be discussed in the next section where we perform a thorough evaluation of the complete system. The geometric representations of ICE are shown in Fig. 3a, b. We will be working in a cylindrical coordinate system with $x \in (0, L)$ being the direction along the cylindrical axis and (r, ϕ) the polar coordinates in the plane perpendicular to it.

2.2 Middle ear system

The main components of the middle ear of lizards are the eardrum, the columella, and the extracolumella. The tympanum, or eardrum, is a thin membrane that separates the outer ear and the middle ear, and vibrates in response to external sound waves. The space on the deep (inner) side of the tympanum is the middle ear cavity; this cavity is linked, by the Eustachian tube, to the larger midline pharyngeal cavity. Unlike humans, lizards possess only a single middle ear bone, the *columella*, that is connected (typically asymmetrically) to the eardrum by means of a cartilaginous element, the *extracolumella*. The placement of the extracolumella can be seen on the left in Fig. 4a.

The membrane-extracolumella-columella system functions as a second-order lever where the internal and external pressures drive the membrane, which in turn causes a displacement of the extracolumella. This motion is transferred via the columella to the inner ear (the perilymphatic fluid of the cochlea). The cochlear hair cells transduce this fluid motion into electrochemical impulses, which will be passed on to the brain via the auditory nerve; cf. Fig. 4b.

For frequencies that are not too high (say, below 4 kHz), the extracolumella can be taken to move as a completely stiff bar. Manley (1972b) has shown that the extracolumella begins to flex at higher frequencies, which is illustrated in Fig. 5. This flexion reduces the columellar transfer efficiency and is partly responsible for the poor high-frequency response of gecko middle ears, a feature also observed in other non-mammalian vertebrates. In our current treatment, however, we assume that the extracolumella behaves as a rigid plate as our frequencies of interest to auditory processsing are <4 kHz.

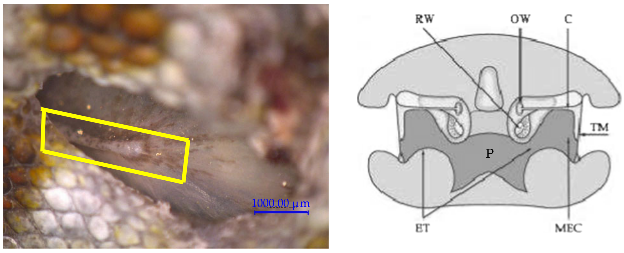

(a) **(b)**

Fig. 4 *Left* close-up shot of a *T. gecko* illustrating the scale and shape of the tympanum and the extracolumella (*red box*). The extracolumella, which is embedded into the tympanic membrane, picks up the membrane vibrations and transmits them through the columella—see also Fig. 5—to the cochlea. Courtesy of Prof. Zhendong Dai (NUAA). *Right* cross section of a lizard's head. The tympanic membranes (TM) as well as the air inside the middle ear cavity (MEC) and eustachian tubes (ET) are excited by incoming sound waves. Because of the large width of the eustachian tubes (ET), the air inside the pharynx (P) is also excited. The tympanic vibration drives the columella (C) in such a way that its lever construction transmits the vibrations to the oval window (OW), the membrane at the entrance to the cochlea. The OW vibration excites the cochlear fluid, giving rise to a frequency-dependent activation of the underlying auditory nerve fibers. The round window (RW) is a membrane that serves to compensate the pressure within the fluid. Figure taken from (Christensen-Dalsgaard and Manley 2005). **a** Gecko eardrum, **b** head cross section (color figure online)

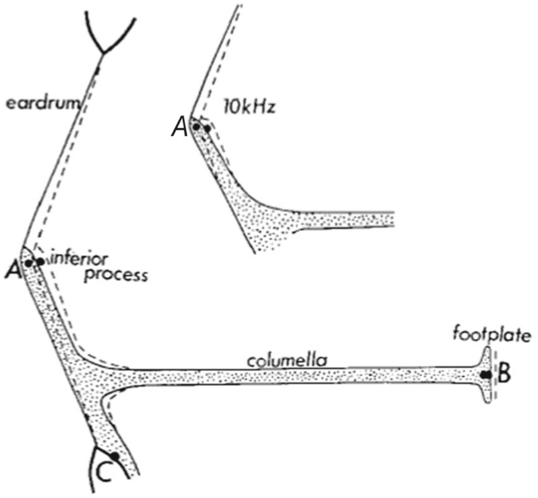

Fig. 5 Operation of the middle ear lever in Geckos reproduced from Manley (1972b). The inferior process of the extracolumella (AC) hinges at point C. At low frequencies, the extracolumella is a stiff bar, but at higher frequencies, the inferior process of the extracolumella begins to flex as shown in the inset. The columellar footplate (B) is a piston that fits into the oval window of the cochlea

2.2.1 *Tympanic membrane*

The extracolumella applies a significant mechanical load to the tympanum (Manley 1972a) precluding its treatment as a freely vibrating membrane. Furthermore, the asymmetric contact of the extracolumella has important physical consequences, especially in the observed vibration patterns of the membrane.

In a previous treatment (Vossen et al. 2010) of ICE, the tympanum was modeled as a clamped circular membrane with asymmetrically attached sectorial load between $-\beta < \phi < \beta$. This manifests itself as an additional boundary condition at $\phi = \beta$ and $\phi = -\beta$ which has to be satisfied via a numerical approximation of keeping the extracolumella straight. In other words, the membrane would be constrained to vibrate with a profile that would best approximate a straight line at the extracolumella boundary. While this method has the advantage of being able to quite accurately reproduce the complex vibration patterns of the eardrum, it does not lend itself well to an analytical treatment of the coupled system.

In our recent model (Vedurmudi et al. 2016), we took a slightly different path. The tympanic membrane will be modeled as a rigidly clamped sectorial membrane with its vibrating part limited to $\beta < \phi < 2\pi - \beta$. This means that in addition to the radial boundary at a_{tymp}, we have a new set of boundaries at $\phi = \beta$ and $\phi = 2\pi - \beta = -\beta$ where the membrane vibration is set to zero. This is illustrated in 6. The membrane material will be assumed to be linear-elastic. As before, the equations describing the vibrations of the membrane will consequently be linear 2nd-order partial differential equations (PDE's) to be derived in Sect. 3.2.

In doing so, the extracolumella is effectively of infinite mass and motionless, a reasonable approximation since the extracolumella and attached proximal elements are typically much heavier than the rest of the membrane. Typically, the mass of an isolated "clean" tympanum is of the order of 1 mg. The mass of the extracolumella, columella, and intimately linked ligaments is about 10× more, and the endolymph directly linked to the columella is 500 mg. Hence, the ratio of tympanic mass to the coupled mass behind it is $<1/300$.

2.3 Head model and sound input

In realistic environments, the acoustic fields experienced by animals are often very complex. In addition to sound waves radiated directly from one or more sources, they also involve waves reflected from objects in their immediate neighborhood. Most mammals possess the neuronal power required to carry out the sophisticated signal processing needed to derive useful information from these signals, whereas animals like geckos respond to simpler cues—usually, the direct field from the nearest or strongest source.

We will therefore model our incoming input as a simple plane wave (or equivalently, a pure tone) of a given frequency. This is not a restriction since the ensuing mathematical description may be taken as linear. The input is specified in terms of its intensity, frequency, and direction. Such a stimulus can be generated experimentally, for instance in an anechoic chamber using loudspeakers that are placed at a distance from the animal that is large compared to the animal's size and the wavelength of the sound involved (Christensen-Dalsgaard and Manley 2005, 2008; Christensen-Dalsgaard et al. 2011). In other experiments, a similar stimulus has also been provided by means of a headphone sealed to the ear (Koeppl and Carr 2008).

The amplitude of the sound pressure on the outer surface of the eardrum can be taken as uniform. The spatial variation can be safely neglected as the typical eardrum is less than 5 mm in diameter, whereas the smallest sound wavelengths in the hearing range of the larger *Varanus* is ∼170 mm (2 kHz) and is around ∼85 mm (4000 Hz) for the smaller *Tokay gecko*. In other experiments, a similar stimulus has also been provided by means of a headphone sealed to the ear (Koeppl and Carr 2008).

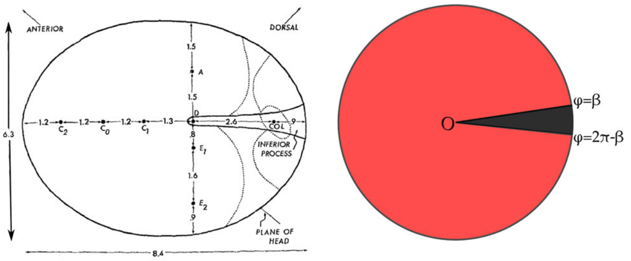

(a) **(b)**

Fig. 6 *Left* sketch of the eardrum of a *T. gecko*, taken from Manley (Manley 1972a). "COL" is the approximate position of the columella on the extracolumellar footplate. Dimensions in millimeters. *Right* the tympanic membrane in ICE. The *lightly shaded* region is modeled as a linear-elastic membrane, whereas the *darkly shaded* region ($\beta < \phi < 2\pi - \beta$) represents the extracolumella, which together with the masses behind it is taken to be infinitely heavy; see main text. The angle β corresponds to the breadth of the extracolumella and is estimated from anatomical data. **a** Gecko eardrum, **b** ICE eardrum

In general, as a result of the diffraction of sound around the head and body of an animal, there would be a difference in phase as well as amplitude between the sound at the two ears. The exact variation depends on the size of the animal and the frequency of the incident wave. However, because of the small interaural lengths (relative to the stimulus wavelength) of many animals with ICE, certainly lizards and frogs, the amplitude difference is negligible (Michelsen and Larsen 2008). The phase difference, although small compared to those in larger animals due to the absence of any significant diffraction, is not negligible. Accordingly, the inputs at both ears have the same amplitude p and a small frequency and direction-dependent phase difference Δ. As we will later see, through ICE, even animals with small interaural distance L can obtain useful internal time and level differences (Fig. 6). The sound inputs to both ears are given by

$$p_0 = p\mathrm{e}^{i\omega t}\mathrm{e}^{ik\Delta/2} \qquad p_L = p\mathrm{e}^{i\omega t}\mathrm{e}^{-ik\Delta/2} \tag{2}$$

$$\Delta = L\sin\theta. \tag{3}$$

We have also chosen a coordinate system relative to the *median-sagittal* plane or the head midline of the animal such that θ gives the angle of incidence of the sound wave relative to this plane. For more complex auditory systems, we would require two angles (θ, ϕ) but this is not needed for our analysis. According our convention, $\theta = 0°$ corresponds to sources directly in front of the animal and $\theta = \pm 180°$ to those directly behind. The ear closer to the sound source is said to be *ipsilateral*, while the one further away from the source is called the *contralateral* ear. The terms ipsi- and contralateral also refer to the stimuli at the respective ears; cf. Fig. 7.

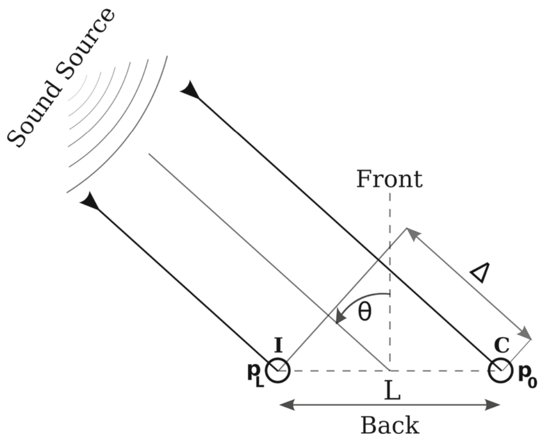

Fig. 7 Acoustic head model for ICE. Depending on the angle of the sound source θ, the distance between the sound source and the contralateral (C) ear is longer than its distance from the ipsilateral (I) ear. The extra distance travelled by the sound wave to reach the contralateral ear is $L \sin\theta$ which gives rise to a phase difference $\Delta = kL\sin\theta$. The small head size of many of these animals lets us safely (Michelsen and Larsen 2008) neglect diffraction effects on the phase and amplitude difference, which would have required us to account for the fact that the sound wave would have to travel around the head to reach the contralateral ear

Given a source direction θ, $\Delta = L\sin\theta$ is the additional distance traveled by the sound wave to reach the contralateral ear (see Fig. 7). We note that in defining the input in this way, we have also emphasized the symmetry of the system.

Table 1 Functions and variables used in the ICE model

θ, ω, k	Sound source direction, angular frequency and wavenumber ($k = \omega/c$) with sound speed $c = 343\,\text{ms}^{-1}$
$p_{0/L},\ \Delta$	Sound pressure inputs to the two ears given the direction and the phase difference between them
$L, a_{\text{cyl}}, V_{\text{cav}}$	Interaural separation (or cylinder length), cylinder radius, cavity volume
$J_{\text{q}}, \mu_{\text{qs}}, \nu_{\text{qs}}$	Order q Bessel function of the first kind, its sth zero and sth extremum, respectively
$p_{\text{qs}}(x, r, \phi), \zeta_{\text{qs}}$	Cavity pressure modes and corresponding axial wavenumbers
$p(x, r, \phi; t), \text{v}_x(x, r, \phi; t)$	Cavity pressure distribution and air velocity
$u_{\text{mn}}(r, \phi; t), \omega_{\text{mn}}$	Tympanic membrane eigenmodes and corresponding eigenfrequencies
$u_{0/L}(r, \phi; t), u^{\text{ave}}_{0/L}(t)$	Membrane displacement—full and average
$\Lambda(\omega)$	Membrane frequency response
$\rho_M, d_M, a_{\text{tymp}}$	Membrane density, thickness and radius
$\beta < \phi < 2\pi - \beta$	Extent of the vibrating part of the membrane. The remaining sector corresponds to the extracolumella
f_0, α	Membrane fundamental frequency and damping coefficient

3 Derivation of the mathematical model

In this section, we will use the physical model for internally coupled ears to derive an expression for the vibrations of the eardrum in terms of the sound input. Our goal is to accurately represent the functions and do so in such a way that the frequency and direction dependence as well as the effects of coupling are apparent. While deriving the main functions of interest, we will also find an expression for the cavity pressure distribution and discuss the appropriate boundary conditions and approximations that relate the membrane vibrations to the internal pressure. In Table 1, the main functions used in the derivation below have been listed, together with their physical interpretation.

In order to motivate the derivation below, we start by briefly discussing the final expression that relates the membrane vibrations to the sound inputs. This also serves to clearly see the interplay between the terms corresponding to the membrane and to the internal cavity. Given a pair of internally coupled tympana of area $\mathscr{S}_{\text{tymp}} = (\pi - \beta)a^2_{\text{tymp}}$ driven by the sound pressures given in (2), the displacement of its surface at a position (r, ϕ) is given by

$$u_{0/L}(r, \phi; \omega, t) = \frac{1}{2}\left(\frac{p_L + p_0}{1 + \Lambda_{\text{tot}}\Gamma_+} \mp \frac{p_L - p_0}{1 + \Lambda_{\text{tot}}\Gamma_-}\right)\Lambda, \quad (4)$$

where

$$\Lambda = \sum_{m,n}^{\infty} \frac{u_{\text{mn}}(r, \phi) \int \text{d}S\, u_{\text{mn}}}{\rho_M d_M \Omega_{\text{mn}} \int \text{d}S\, u^2_{\text{mn}}}, \quad (5)$$

$$\Lambda_{\text{tot}}(\omega) = \int_{S_{\text{mem}}} \text{d}S\ \Lambda(r, \phi, \omega)\,, \quad (6)$$

$$\Gamma_+ = -\frac{\rho c^2}{V_{\text{cav}}} kL \cot kL/2, \qquad \Gamma_- = \frac{\rho c^2}{V_{\text{cav}}} kL \tan kL/2. \quad (7)$$

Here $\Omega_{\text{mn}} = \omega^2 - \omega^2_{\text{mn}} - 2i\alpha\omega_{\text{mn}}$ and the integrals are taken over the vibrating part membrane surface,

$$S_{\text{mem}} = (r, \phi) \in \left(0, a_{\text{tymp}}\right) \times (\beta, 2\pi - \beta)\,.$$

The membrane eigenmodes, denoted by u_{mn}, can be explicitly written down as

$$u_{\text{mn}}(r, \phi) = \sin\kappa(\phi - \beta) J_\kappa(\mu_{\text{mn}} r), \quad (8)$$

where $\kappa[m] = \frac{m\pi}{2(\pi-\beta)}$, $m = 1, 2, 3, \ldots$ and J_κ is the order-κ Bessel function of the first kind with $\mu_{\text{mn}} \times a_{\text{tymp}}$ being its nth zero. The remaining quantities are defined in Table 1.

For a solitary driving pressure $pe^{i\omega t}$ on an individual membrane's surface, $\Lambda(r,\phi) = u(r,\phi)/p$ is its frequency response and Λ_{tot} is the integral of Λ over the vibrating part of the membrane surface S_{mem}. The frequency dependence of both these terms is contained in Ω_{mn} which will be defined later; cf. (47). In (7), $\Gamma_{\pm}$ corresponds to the frequency response of the internal cavity. Readers who want to skip the mathematical details, can continue with the next section.

3.1 Cavity pressure

At our frequencies of interest (<4 kHz), viscous acoustic damping in air can be neglected so that we follow common acoustic models (Rschevkin 1963; Temkin 1981; Fletcher 1992) and describe the air inside the cavity by linear acoustics in a cylindrical coordinate system. In this approach, air moves due to a local pressure $p(x,r,\phi;t)$ obeying the three-dimensional wave equation

$$\frac{1}{c^2}\frac{\partial^2 p(x,r,\phi;t)}{\partial t^2} = \Delta_{(2)}\,p(x,r,\phi;t) + \frac{\partial^2 p(x,r,\phi;t)}{\partial x^2} \tag{9}$$

where

$$\Delta_{(2)} = \frac{1}{r}\frac{\partial}{\partial r} + \frac{\partial^2}{\partial r^2} + \frac{1}{r^2}\frac{\partial^2}{\partial \phi^2} \tag{10}$$

is the two-dimensional Laplacian in polar coordinates and c is speed of sound. The complete solution must take into account the boundary conditions at and within the cavity walls and the ones at the air–membrane interface. We also note that Eq. (9) presumes through its boundary conditions that the animal's mouth is closed, which is typical for a waiting predator or prey.

In order to solve (9) for a particular frequency f with angular frequency $\omega = 2\pi f$, we use the following separation ansatz[1]

$$p(x,r,\phi,t) = f(x)g(r)h(\phi)\exp(i\omega t) \tag{11}$$

which after substitution into (9) leads to,

$$\begin{aligned} &k^2 f(x)g(r)h(\phi) + f(x)h(\phi)\left[\frac{\partial^2 g(r)}{\partial r^2} + \frac{1}{r}\frac{\partial g(r)}{\partial r}\right] \\ &\quad + f(x)g(r)\frac{1}{r^2}\frac{\partial^2 h(\phi)}{\partial \phi^2} + g(r)h(\phi)\frac{\partial^2 f(x)}{\partial x^2} = 0. \end{aligned} \tag{12}$$

As always, $k := \omega/c$ is the wavelength of the sound wave at the given angular frequency ($\omega = 2\pi f$). The substitution $\exp(i\omega t)$ in (11) actually means that we are looking for the (countable) eigenvalues of $-\Delta$ inside the cavity, in terms of ω^2 with appropriate boundary conditions; see below. Although this might look mathematically contradictory at first, we will soon see that it is not. Making the ansatz of separation of variables and dividing (12) by $f(x)g(r)h(\phi)$ gives the following set of separated ordinary differential equations (ODEs),

$$\frac{d^2 f(x)}{dx^2} + \zeta^2 f(x) = 0 \tag{13}$$

$$\frac{d^2 h(\phi)}{d\phi^2} + q^2 h(\phi) = 0 \tag{14}$$

$$\frac{\partial^2 g(r)}{\partial r^2} + \frac{1}{r}\frac{\partial g(r)}{\partial r} + \left[\left(\underbrace{k^2 - \zeta^2}_{=:\nu_{\mathrm{q}}^2}\right) - \frac{q^2}{r^2}\right] g(r) = 0 \tag{15}$$

with separation constants q and ζ. The first two equations are second-order ODEs that can be readily solved to give,

$$f(x) = \exp\left(\pm i\zeta x\right) \tag{16}$$

$$h(\phi) = \exp\left(\pm i q\phi\right). \tag{17}$$

The third Eq. (15) is known as the Bessel differential equation (Copson 1973, p. 313) and its general solution is given by

$$g(r) = C_{\mathrm{q}} J_{\mathrm{q}}\left(\nu_{\mathrm{q}} r\right) + D_{\mathrm{q}} Y_{\mathrm{q}}\left(\nu_{\mathrm{q}} r\right). \tag{18}$$

J_{q} and Y_{q} are the order-q Bessel functions of the first and second kind, respectively. We can set the coefficients $D_{\mathrm{q}} = 0$ as the Bessel function of the second kind diverges at $r = 0$ (Copson 1973), and we are seeking solutions that remain finite on the membrane surface.

With the above solutions for $f(x)$, $g(r)$, and $h(\phi)$, we can write down a specific solution to (9),

$$p_{\mathrm{q}}(x,r,\phi) = \left(A_{\mathrm{q}}\exp(i\zeta_{\mathrm{q}}x) + B_{\mathrm{q}}\exp(-i\zeta_{\mathrm{q}}x)\right) p_{\mathrm{q}}^{\circ}(r,\phi) \tag{19}$$

$$p_{\mathrm{q}}^{\circ}(r,\phi) = J_{\mathrm{q}}(\nu_{\mathrm{q}} r/a_{\mathrm{cyl}})\left(C_{\mathrm{q}}\cos q\phi + D_{\mathrm{q}}\sin q\phi\right). \tag{20}$$

The coefficients A, B, q, ζ, and ν will be subsequently determined by the boundary conditions. Through p_{q}°, we denote the components of the eigenfunction in the radial and azimuthal directions.

3.1.1 Pressure boundary conditions

In order to determine the coefficients in (20), we have to satisfy three sets of boundary conditions,

---

[1] Before proceeding we should note that in general, the time component of the pressure also has a temporally *backward-moving* component, i.e., $\exp(-i\omega t)$. By making the ansatz in (11), we have implicitly used the fact that the form of the input as given in (2) constrains the pressure to only having a *forward-moving* component, i.e., $\exp(i\omega t)$. As for the separation ansatz, the reader may well consult Asmar (2005, p. 187).

- Continuity and smoothness in ϕ or equivalently $h(0) = h(2\pi)$ and $\left.\frac{\mathrm{d}h}{\mathrm{d}\phi}\right|_{\phi=0} = \left.\frac{\mathrm{d}h}{\mathrm{d}\phi}\right|_{\phi=2\pi}$
- Vanishing of the normal derivative at the cavity walls—$\left.\frac{\mathrm{d}g}{\mathrm{d}r}\right|_{r=a_{\mathrm{cyl}}} = 0$.
- Equating the membrane velocity to the air velocity at the inner air–membrane interface.

The first set of requirements is trivial and constrains q to take integer values. The second and third are a result of the so-called “no-penetration” boundary condition of fluid mechanics. They arise from the fact that the cavity wall is an impermeable boundary. This translates into the requirement that the normal velocity function should vanish (Pozrikidis 2009, p. 111). The velocity function ($\mathbf{v}$) is related to the pressure by

$$-\rho\frac{\partial \mathbf{v}}{\partial t} = \nabla p. \tag{21}$$

where ρ is the density of air. This result emerges directly from the linearization of the Euler equation

$$\frac{\partial \tilde{\mathbf{v}}}{\partial t} + \tilde{\mathbf{v}}.\nabla\tilde{\mathbf{v}} = -\frac{1}{\rho}\nabla P + \mathbf{f}. \tag{22}$$

Assuming that the acoustic pressure can be described as a fluctuation p around a stationary background (atmospheric) pressure P_0 and that the fluid velocity $\mathbf{v}$, as small fluctuations in a quiescent fluid $\mathbf{v}_0 = 0$, we obtain

$$\tilde{\mathbf{v}} = \mathbf{v}_0 + \mathbf{v} = \mathbf{v}$$
$$P = P_0 + p.$$

Neglecting the body forces due to gravity ($\mathbf{f}$) gives us

$$\Rightarrow \frac{\partial \mathbf{v}}{\partial t} + (\mathbf{v}\cdot\nabla)\mathbf{v} = -\frac{1}{\rho}\nabla p. \tag{23}$$

We can neglect the convection term $(\mathbf{v}\cdot\nabla\mathbf{v})$ as it is of second order in the extremely small $\mathbf{v}$, and thus arrive at (21).

At the cylindrical cavity wall, the normal velocity is in the radial direction and vanishes. Substituting the expression (25) for the pressure into (21) leads to a Neumann boundary condition for the pressure,

$$\mathrm{v}_r = -\frac{1}{i\rho\omega}\left.\frac{\partial p(x,r,\phi;t)}{\partial r}\right|_{r=a_{\mathrm{cyl}}} = 0$$
$$\Rightarrow \left.\frac{\partial J_{\mathrm{q}}(\nu_{\mathrm{q}} r)}{\partial r}\right|_{r=a_{\mathrm{cyl}}} = 0 \tag{24}$$

This constrains ν_{q} to a discrete set of values which correspond to the local minima and maxima of J_{q}. We therefore introduce an additional index s which takes integer values such that $\nu_{\mathrm{qs}} \times a_{\mathrm{cyl}}$ corresponds to the sth extremum of the order-q Bessel function of the first kind. This results in (19) becoming a set of modes indexed by (q, s):

$$p_{\mathrm{qs}}(x,r,\phi) = \left(A_{\mathrm{qs}}\exp(i\zeta_{\mathrm{qs}}x) + B_{\mathrm{qs}}\exp(-i\zeta_{\mathrm{qs}}x)\right)p^{\circ}_{\mathrm{qs}} \tag{25}$$
$$p^{\circ}_{\mathrm{qs}}(r,\phi) = J_{\mathrm{qs}}(\nu_{\mathrm{qs}}r/a_{\mathrm{cyl}})\left(C_{\mathrm{qs}}\cos q\phi + D_{\mathrm{qs}}\sin q\phi\right). \tag{26}$$

Effectively, the modes are three-dimensional waves propagating with wave numbers ζ_{qs} in the x-direction and ν_{qs} in the radial direction. The first of these modes (corresponding to $q = 0, s = 0$) is of particular importance. Since the first maximum of J_0 occurs at $r = 0$, we have $\nu_{00} = 0$. This leads to the first mode being a plane wave that is constant in r and ϕ and only propagates along the axis of the cylinder.

The modes defined through (19) and (24) form a discrete orthogonal basis inside the cylinder. This means that

$$\int_{\Omega}\mathrm{d}V\,p_{q_1 s_1}p_{q_2 s_2} = 0, \quad \text{if} \quad q_1 \neq q_2 \quad \text{or} \quad s_1 \neq s_2 \tag{27}$$

where the integral is over the volume of the cylinder. This is a consequence of the fact that for different q’s the trigonometric parts of the modes are orthogonal, whereas for the same q the Bessel parts are orthogonal for different s’s. Expressed mathematically, this requirement gives us

$$\int \mathrm{d}S\; f_{q_1 s_1}f_{q_2 s_2} = 0, \quad q_1 \neq q_2 \quad \text{or} \quad s_1 \neq s_2 \tag{28}$$

where $\mathrm{d}S = r dr d\phi$ with the integral being taken over the disk of radius a_{cyl}. We can therefore write the general solution to (9) as a linear combination of the orthogonal modes given in (25):

$$p(x,r,\phi;t) = \sum_{q=0}^{\infty}\sum_{s=0}^{\infty}p_{\mathrm{qs}}(x,r,\phi)\mathrm{e}^{i\omega t} \tag{29}$$

where the individual modes p_{qs} are defined in (19).

The third and final set of boundary conditions at the internal air–membrane interface at either end of the cylinder will be used to determine the remaining coefficients, A_{qs} and B_{qs}. To do so, we first need to find an analytical expression for the membrane vibrations.

3.2 Tympanic vibrations

The eardrum is modeled as a damped linear-elastic membrane obeying

$$-\frac{\partial^2 u}{\partial t^2} - 2\alpha\frac{\partial u}{\partial t} + c_M^2\Delta_{(2)}u = \frac{1}{\rho_M d_M}\Psi(r,\phi;t) \tag{30}$$

with displacement $u(r, \phi; t)$, damping coefficient α, density ρ_M, thickness d_M, and wave-propagation velocity

$$c_M = \sqrt{T_0/\rho_M} \tag{31}$$

(cf. Table 1) where T_0 is the membrane tension. Furthermore, $\Psi(r, \phi; t)$ is the total pressure driving the membrane (on both the inner and the outer surface). The tympanic membrane is fixed at its radial boundary $r = a_{\text{tymp}}$ and, as a consequence of the presence of the extracolumella, at $\phi = \pm\beta$.

As a preliminary exercise, we first derive expressions for the free and force-driven vibrations of a circular membrane. We will then use our results to move on to the sectorial membrane which corresponds to the tympanum loaded by the extracolumella.

3.2.1 Circular membrane

We consider a rigidly clamped circular membrane of radius a_{tymp} and solve for the membrane displacement $u(r, \phi)$ at a point (r, ϕ) with $r < a_{\text{tymp}}$ and $0 \leq \phi < 2\pi$. Due to the absence of the extracolumella, the membrane is only subject to the Dirichlet boundary condition $u(r, \phi; t)|_{r=a_{\text{tymp}}} = 0$.

We first determine the eigenmodes of an undamped circular membrane by solving (30) for $\alpha = 0,\ \Psi = 0$. We solve the resulting two-dimensional Helmholtz equation by using a separation ansatz, similar to the one used in (11),

$$u(r, \phi; t) = f(r)g(\phi)T(t). \tag{32}$$

This gives us the following set of equations

$$\frac{d^2 g(\phi)}{d\phi^2} + m^2 g(\phi) = 0 \tag{33}$$

$$\frac{d^2 T(t)}{dt^2} + c_M^2 \mu^2 T(t) = 0 \tag{34}$$

$$\frac{\partial^2 f(r)}{\partial r^2} + \frac{1}{r}\frac{\partial f(r)}{\partial r} + \left[\mu^2 - \frac{m^2}{r^2}\right] f(r) = 0 \tag{35}$$

with separation constants μ and m. The above equations are identical to those in (13)–(15). The solution to (35) is, as before, $J_m(\mu r)$, the order-m Bessel function of the first kind (Copson 1973). The boundary condition in the ϕ direction remains the same resulting in

$$u_{\text{mn}}^{\text{circ}}(r, \phi; t) = \left(E_{\text{mn}} e^{i\omega_{\text{mn}} t} + F_{\text{mn}} e^{-i\omega_{\text{mn}} t}\right) u_{\text{mn}}^{\text{circ}}(r, \phi) \tag{36}$$

$$u_{\text{mn}}^{\text{circ}}(r, \phi) = [M_{\text{mn}} \cos m\phi + N_{\text{mn}} \sin m\phi]\, J_m(\mu_{\text{mn}} r). \tag{37}$$

In contrast to the boundary condition for the pressure in the internal cavity (24), we require u to vanish at the boundary. In other words, we impose a Dirichlet boundary condition which effectively requires $J_m(\mu a_{\text{tymp}}) = 0$. This constrains μ to a discrete set of values which correspond to the zero of J_m. In (37), the combination of a_{tymp} and μ_{mn} corresponds to the nth zero of J_m and $\omega_{\text{mn}} = c_M \mu_{\text{mn}}$ is the eigenfrequency of the (m, n) eigenmode.

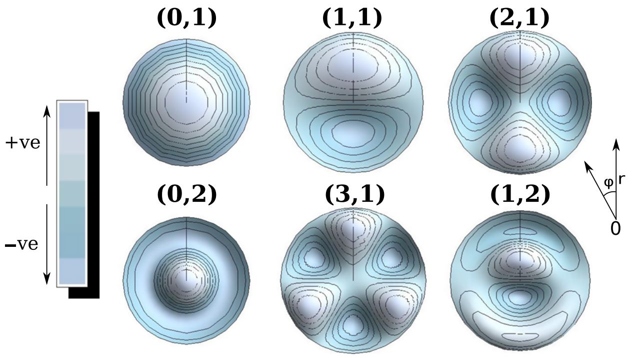

Fig. 8 Eigenmodes of a full circular membrane with the characteristic numbers of the modes shown above each figure. Displacements into the surface of the paper are *darkly shaded*, while those out are lightly shaded (illustrated in the legend). The eigenfrequency increases from *left* to *right* and *top* to *bottom*. This kind of a vibration profile does not agree well with that for lizards due to the asymmetry brought about by the embedded extracolumella (see next subsection), but does agree fairly well for frogs since their extracolumella is attached symmetrically to the middle of the tympanum (Jørgensen 1993); see also Fig. 9

In general, m can take any positive real value—a fact that will help us solve the sectorial membrane problem. In the case of a full circular membrane, however, as in the case of the pressure inside a cylindrical cavity, requirements of continuity and smoothness in ϕ result in m taking integer values only. Moreover, the eigenmodes also form an orthogonal set. For later convenience, we denote the spatial part of the above mode by $u_{\text{mn}}^{\text{circ}}(r, \phi)$. The first few of these modes have been plotted in Fig. 8. We also note that a freely vibrating membrane can have time-dependent components that are both forward- and backward-moving. The presence of a driving force, however, will result in familiar expressions.

3.2.2 Sectorial membrane

In Sect. 2.2.1, we noted that in vertebrates there is a transducer for the membrane's vibrations in the form of an asymmetrically attached extracolumella. Consequently, the membrane cannot be modeled as a full circular disk, but rather as a sector of a given angle. For such a membrane, the equation of motion of the vibrating part remains unchanged. However, because of its odd shape, we now have a new set of temporally fixed boundary conditions at $\phi = \beta$ and $\{\phi = 2\pi - \beta = -\beta, 0 \leq re a_{\text{tymp}}\}$, in addition to the one at $r = a_{\text{tymp}}$. In order to calculate the eigenmodes, we proceed from the definition in (37) and determine the values that m is constrained to take based on the boundary conditions at all three edges of the extracolumella.

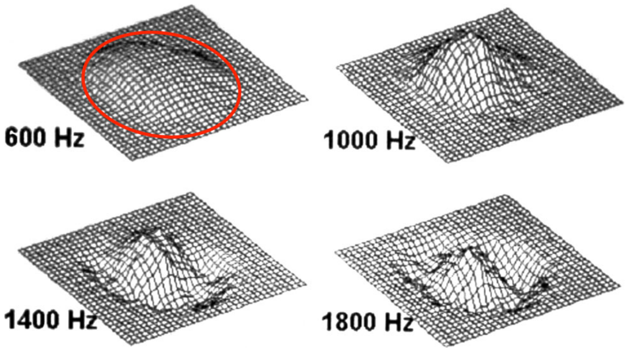

Fig. 9 The extracolumella touches the circular eardrum of frogs in the middle, hence not breaking its rotational symmetry. The above plots show unpublished experimental results of Jørgensen (1993) on excitation patterns of the tympanum for different frequencies, as indicated. They all look rotationally invariant. The fixed, circular, border has been indicated once by a *solid* (*red*) *circle* for 600 Hz. The dominant mode for 600 Hz is the fundamental one (0,1), higher modes mix in as the frequency increases, corresponding nicely to the Bessel function of the mode (0, 2); cf. Fig. 8. Plot courtesy of Jørgensen (color figure online)

We also note that because of the relatively large mass of the extracolumella as well as its attached elements in comparison to the membrane, we can effectively model it as an infinitely heavy sectorial plate. As a result we require that the membrane displacement goes to zero at $\phi = \beta$ and $\phi = 2\pi - \beta$ so that the ϕ part of (37) takes the form $\sin \kappa(\phi - \beta)$. We therefore obtain the following set of orthogonal eigenmodes,

$$u_{\mathrm{mn}}(r, \phi; t) = \left[M_{\mathrm{mn}} \mathrm{e}^{i\omega_{\mathrm{mn}}t} + N_{\mathrm{mn}} \mathrm{e}^{-i\omega_{\mathrm{mn}}t}\right] u_{\mathrm{mn}}(r, \phi) \quad (38)$$

$$u_{\mathrm{mn}}(r, \phi) = \sin \kappa(\phi - \beta) J_{\kappa}(\mu_{\mathrm{mn}} r) \quad (39)$$

where $\kappa[m] = .5\, m\pi/(\pi - \beta)$, $m = 1, 2, 3, \ldots$. We see that the radial—r—part of the above mode is given by the order-κ Bessel function of the first kind with $\mu_{\mathrm{mn}} \times a_{\mathrm{tymp}}$ being its nth zero. The solution for the damped membrane follows in a similar way.

It is apparent from the form of the above modes that unlike in the case of the circular membrane eigenmodes, these modes are no longer symmetric. The sectorial shape of the membrane has important physical consequences and captures the complex vibration patterns of a realistic membrane. For a circular membrane driven by a uniform pressure, the asymmetric modes (with $m \neq 0$) are suppressed. This holds in the case of frogs (Jørgensen and Kanneworff 1998), where the extracolumella is attached to the middle of the tympanic membrane and its rotational symmetry is not broken; see also Fig. 9.

On the other hand, for the sectorial membrane as in the case of lizards, the radial symmetry is broken explicitly by the extracolumella. The first few of these modes are shown in Fig. 10. The vibrations of a sectorial membrane are discussed in more detail in Fletcher (1992, p. 87).

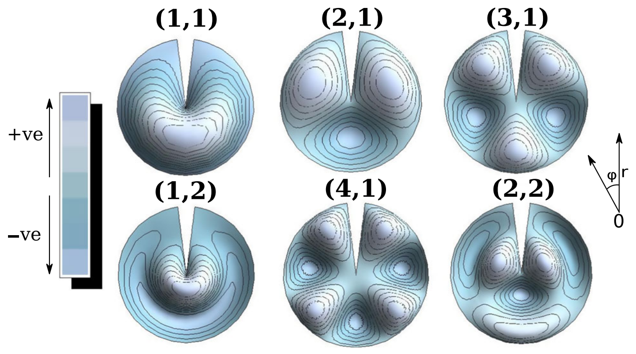

Fig. 10 Eigenmodes of a sectorial membrane where the omitted region corresponds to the extracolumella with $\beta = \pi/25$; cf. Fig. 6b. The eigennumbers are shown above each figure. As in Fig. 8, displacements into the surface of the paper are *darkly shaded* while those out are *lightly shaded*. The eigenfrequency increases from *left* to *right* and *top* to *bottom*

3.2.3 Undamped and damped vibrations

For a damped membrane with $\alpha > 0$ in Eq. (30), the spatial part of the above eigenmodes remains unchanged. The form of the time-dependent part $T(t)$ as given by (32) is obtained from the solution to the following ordinary differential equation,

$$\frac{d^2 h_{\mathrm{mn}}(t)}{\mathrm{d}t^2} - 2\alpha \frac{\mathrm{d}h_{\mathrm{mn}}(t)}{\mathrm{d}t} - \omega_{\mathrm{mn}}^2 h_{\mathrm{mn}}(t) = 0. \quad (40)$$

The above expression differs from the equation for the time-varying part of the pressure (34) only in a first-order damping term. We therefore expect (40) to have exponentially decaying solutions in time and look for them.

As an ansatz, we assume h_{mn} to take the form $\exp(i\widetilde{\omega}_{\mathrm{mn}})$ where $\widetilde{\omega}_{\mathrm{mn}}$ can, in general, be a complex number. This leads to a quadratic equation in $\widetilde{\omega}_{\mathrm{mn}}$ with solutions

$$\widetilde{\omega}_{\mathrm{mn}}^2 - 2i\alpha\widetilde{\omega}_{\mathrm{mn}} - \omega_{\mathrm{mn}}^2 = 0 \quad (41)$$

$$\widetilde{\omega}_{\mathrm{mn}} = i\alpha \pm \omega_{\mathrm{mn}}^* \quad (42)$$

where

$$\omega_{\mathrm{mn}}^* = \sqrt{\alpha^2 + \omega_{\mathrm{mn}}^2}. \quad (43)$$

We see that the new, now damped, eigenmodes possess both an exponential damping term as well as a shift in the original eigenfrequencies. We require the membrane displacement to remain finite as $t \to \infty$. As $\exp(-i\widetilde{\omega}_{\mathrm{mn}})$ terms lead to vibration amplitudes that increase exponentially as $\exp(\alpha t)$ we can safely drop them. This then leads to

$$\widetilde{u}_{\mathrm{mn}}(r, \phi; t) = u_{\mathrm{mn}}(r, \phi) \left[M_{\mathrm{mn}} \mathrm{e}^{i\omega_{\mathrm{mn}}^* t} + N_{\mathrm{mn}} \mathrm{e}^{-i\omega_{\mathrm{mn}}^* t}\right] \mathrm{e}^{-\alpha t}. \quad (44)$$

The effect of membrane damping is therefore not only an exponentially decreasing damping term, but also a shift in the eigenfrequencies of all the membrane eigenmodes. The general solution is given by a linear combination of u_{mn} with the coefficients that are determined by initial conditions. These could be, for instance, membrane displacement and velocity at $t = 0$.

3.2.4 Forced vibrations

For a periodically driven membrane, there are two components of the full solution corresponding to forced vibrations. The first of these is the quasi-stationary-state solution which oscillates with the same frequency as the input and does not depend on the initial conditions—u_{ss}. The second of these is the transient solution that depends on the initial conditions but not directly on the driving pressure—u_t.

The quasi-steady-state solution is expressed as a linear combination of the spatial part of the membrane eigenmodes defined in (39) with a time component equal to that of the driving pressure, $\exp(i\omega t)$,

$$u_{\mathrm{ss}}(r,\phi;t) = \sum_{m=0}^{\infty}\sum_{n=1}^{\infty} C_{\mathrm{mn}} u_{\mathrm{mn}}(r,\phi)\mathrm{e}^{i\omega t}. \tag{45}$$

By substituting (45) into (30) with $\Psi = p\mathrm{e}^{i\omega t}$ we obtain

$$\sum_{m=0}^{\infty}\sum_{n=1}^{\infty} \rho_M d_M \Omega_{\mathrm{mn}} C_{\mathrm{mn}} u_{\mathrm{mn}}(r,\phi)\mathrm{e}^{i\omega t} = p\mathrm{e}^{i\omega t} \tag{46}$$

$$\Omega_{\mathrm{mn}} = \left[\left(\omega^2 - \omega_{\mathrm{mn}}^2\right) - 2i\alpha\omega\right]. \tag{47}$$

Using the orthogonality of the eigenmodes, we can calculate the coefficients C_{mn},

$$C_{\mathrm{mn}} = \frac{p\int \mathrm{d}S u_{\mathrm{mn}}}{\rho_M d_M \Omega_{\mathrm{mn}} \int \mathrm{d}S\,(u_{\mathrm{mn}})^2} \tag{48}$$

with the integral this time being taken over the circular disk of radius a_{tymp} (or equivalently, over the vibrating surface of the tympanum).

The transient solution is found by solving the membrane equation for $\Psi(r,\phi;t) = 0$ which, effectively, is the solution of the free damped membrane, i.e., a linear combination of the eigenmodes given in (44),

$$u_t(r,\phi;t) = \sum_{m=0}^{\infty}\sum_{n=1}^{\infty} \widetilde{u}_{\mathrm{mn}}(r,\phi;t). \tag{49}$$

The complete solution is given by $u = u_t + u_{\mathrm{ss}}$ and the coefficients M_{mn} and N_{mn} are determined by the initial conditions (at $t = 0$).

Quasi-steady-state approximation: the damping coefficient α is usually given in terms of the membrane fundamental frequency (f_0) and a quality factor Q as $\alpha = 2\pi f_0/2Q$. The eardrums in the animals we are concerned with are generally underdamped, i.e., $Q > .5$, which results in damping coefficients that are around ~2600 s^{-1} for the Gecko lizards and around ~400 s^{-1} for the larger Varanids. As a result of the exponential decay of the transient vibration amplitude, we can safely assume that within a few time-periods of the input frequency, and even far less for the Geckos, the transient vibrations of the forced membrane are gone. In our subsequent derivations, we can safely neglect the transient parts of the membrane vibration. The latter will be treated in full elsewhere (Heider et al. 2016).

3.3 Vibration of coupled membranes

We can now move on to the analysis of the vibration of *internally* coupled membranes and derive the expressions defined in (4). The analysis in this section is similar to the treatment of the vibration of a circular membrane backed by a cylindrical air cavity closed at the opposite end as given by (Rajalingham and Bhat 1998). The quantities of interest there were the eigenmodes of the circular membrane, but we are primarily interested in the steady state vibration of sectorial membranes that are internally coupled to each other as well as to external stimuli at both ends.

It is convenient to first write down the main equations of the system based on our previously derived expressions. A general expression for the quasi-steady-state vibrations of the eardrums is given by a linear combination of the sectorial eigenmodes, (39),

$$u_{0/L}(r,\phi;t) = \sum_{m=0}^{\infty}\sum_{n=1}^{\infty} C_{\mathrm{mn}}^{0/L} u_{\mathrm{mn}}(r,\phi)\mathrm{e}^{i\omega t} \tag{50}$$

where 0 and L denote the $x = 0$ and $x = L$ membranes, respectively. Given the cavity pressure distribution $p(x,r,\phi;t)$ as given by (29), the driving pressure on either side of the membrane equals $\Psi^{0/L}(r,\phi;t) = p_{0/L}\mathrm{e}^{i\omega t} - p(0/L,r,\phi;t)$. Substituting these expressions into (30) gives us the following set of equations,

$$\sum_{m=0}^{\infty}\sum_{n=1}^{\infty} \rho_M d_M \Omega_{\mathrm{mn}} C_{\mathrm{mn}}^{0/L} u_{\mathrm{mn}}(r,\phi)\mathrm{e}^{i\omega t} = \Psi^{0/L}(r,\phi;t) \tag{51}$$

The above equation is only valid on the vibrating part of the membrane surface, i.e., for $S_{\mathrm{memb}} = \{r < a_{\mathrm{tymp}}$ and $\beta < \phi < 2\pi - \beta\}$.

As discussed in Sect. 3.1.1, the internal cavity pressure satisfies the no-penetration condition at solid boundaries. This means that at both ends of the cylinder, we equate the velocity profile of air to the velocity profile of the circular surface *including* the membrane; cf. Fig. 11a. As the membrane diameter is smaller than the cylinder diameter, we will have to set the air-particle velocity to zero for $r > a_{\mathrm{tymp}}$. Additionally, since the membrane displacement is only in the x-direction, we need only calculate the x-component of the velocity. Using the relation in (21) we get,

$$\mathrm{v}_{\mathrm{qs}}(x,r,\phi) = \zeta_{\mathrm{qs}}\left(A_{\mathrm{qs}}\mathrm{e}^{i\zeta_{\mathrm{qs}}x} - B_{\mathrm{qs}}\mathrm{e}^{-i\zeta_{\mathrm{qs}}x}\right) p_{\mathrm{qs}}(r,\phi) \tag{52}$$

$$\mathrm{v}_x(x,r,\phi;t) = \frac{-1}{\rho\omega}\sum_{q=0}^{\infty}\sum_{s=0}^{\infty}\mathrm{v}_{\mathrm{qs}}(x,r,\phi)\mathrm{e}^{i\omega t} \tag{53}$$

and the exact boundary conditions are given by

$$\mathrm{v}_x(0,r,\phi;t) = \begin{cases} -i u_0, & (r,\phi)\in S_{\mathrm{memb}} \\ 0, & \text{otherwise} \end{cases} \tag{54}$$

$$\mathrm{v}_x(L,r,\phi;t) = \begin{cases} i u_0, & (r,\phi)\in S_{\mathrm{memb}} \\ 0, & \text{otherwise} \end{cases}. \tag{55}$$

where according to our convention, membrane displacements outward from the cylinder are taken as positive (in x) and those inward are taken as negative.

3.3.1 Approximate boundary condition

As we have just seen, the exact boundary conditions would require us to set the air velocity to be exactly equal to the membrane velocity. However, the membrane and cavity modes are not orthogonal to each other. In other words, each membrane mode couples with every cavity mode and vice versa. Our way around this problem is to approximate the boundary conditions (54) and (55). We do this by effectively replacing each membrane by a circular piston operating on the internal pressure p and moving with the membrane's average velocity $\dot{u}_{0/L}^{\mathrm{ave}}$ so that

$$u_{0/L}^{\mathrm{ave}} = \frac{1}{\pi a_{\mathrm{cyl}}^2}\int \mathrm{d}S\, u_{0/L}\,, \qquad \dot{u}_{0/L}^{\mathrm{ave}} = i\omega u_{0/L}^{\mathrm{ave}} \tag{56}$$

$$\mathrm{v}_x(0,r,\phi;t) = -\dot{u}_0^{\mathrm{ave}}, \qquad \mathrm{v}_x(L,r,\phi;t) = \dot{u}_L^{\mathrm{ave}} \tag{57}$$

where we have in fact taken the average velocity of the entire cylindrical surface including the eardrum; cf. Fig. 11b. Averaging over the tympana is what we call the *piston approximation*. Its mathematical justification is somewhat too involved for the present context and will be presented elsewhere (Heider et al. 2016). Since the bare cylinder surface is solid and nonmoving, the present approximation of averaging over the lateral faces of the cylinder only differs from the average over the membrane surface by a factor.

Physically, one can imagine air as "pretty" incompressible so that in the long-wavelength domain we focus here a local boundary variation on one or both faces (corresponding to the membrane displacement) has the same effect as the average variation on the left and right face from where it propagates through the cylinder representing the pharyngeal cavity. As said in the caption of Fig. 11b, "In effect, it computes the net volume change," as confirmed mathematically (Heider et al. 2016)

$$\Delta V_{\mathrm{cav}} = \pi a_{\mathrm{cyl}}^2\left(u_L^{\mathrm{ave}} + u_0^{\mathrm{ave}}\right).$$

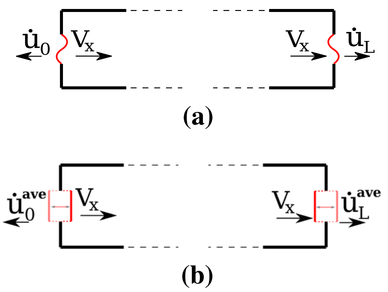

Fig. 11 *Above* exact membrane boundary conditions. The velocity of air (v_x) equals that of the membrane ($u_{0/L}$). *Below* piston approximation. The membrane is approximated by a circular piston moving with the membrane's average velocity and with boundary conditions (57) applied to (9) and (21). The piston approximation refers to (9) and the boundary condition for the pressure p in the 3-dimensional cavity, not to the motion (30) of the eardrum itself. In effect, it computes the net volume change, **a** exact membranes, **b** piston approximation

Even in the absence of the extracolumella with full circular membranes on either end of the cylinder and despite being in different dimensions (2 and 3), the cavity and membrane modes have different boundary conditions. These are Neumann for the cavity boundaries, incl. time-varying ones if a sound stimulus is present at the tympana, and Dirichlet for the membranes clamped at their borders.

Given the modified boundary conditions (57), it is straightforward to calculate the coefficients A_{qs} and B_{qs} in terms of $u_{0/L}^{\mathrm{ave}}$. To do this, we use the orthogonality of the cavity modes (27) and the modal expansion (52), (53) of the air velocity. By multiplying both sides of the boundary relations in (57) by $p_{\mathrm{qs}}(r,\phi)$ and integrating over the circular surfaces at the ends of the cylinder, this results in a system of two linear equations for each pair of A_{qs} and B_{qs},

$$A_{\mathrm{qs}} - B_{\mathrm{qs}} = -L_{\mathrm{qs}}\rho\omega^2 u_0^{\mathrm{ave}} \tag{58}$$

$$A_{\mathrm{qs}}\mathrm{e}^{i\zeta_{\mathrm{qs}}L} - B_{\mathrm{qs}}\mathrm{e}^{-i\zeta_{\mathrm{qs}}L} = L_{\mathrm{qs}}\rho\omega^2 S_L^{\mathrm{ave}} \tag{59}$$

where

$$L_{\mathrm{qs}} = \frac{\int \mathrm{d}S p_{\mathrm{qs}}(r,\phi)}{i\zeta_{\mathrm{qs}}\int \mathrm{d}S p_{\mathrm{qs}}^2(r,\phi)}. \tag{60}$$

We must now make use of the fact that the cavity pressure modes (25) integrate to 0 (i.e., $\int \mathrm{d}S p_{\mathrm{qs}} = 0$) unless $q = 0$

and $s = 0$. For $q = 0$, this is a consequence of the Bessel functions integrating to zero, while for $q \geq 1$, this is due to the more obvious fact that the integral of the trigonometric part from 0 to 2π is zero. That is,

$$\int_0^{a_{\text{acyl}}} r J_{\text{q}}(\nu_{\text{qs}} r) \mathrm{d}r = 0, \tag{61}$$

$$\int_0^{2\pi} \left(A_{\text{qs}} \cos q\phi + B_{\text{qs}} \sin q\phi \right) \mathrm{d}\phi = 0. \tag{62}$$

As a result we have $A_{\text{qs}} = B_{\text{qs}} = 0$ for all modes except the $(0, 0)$ mode. In other words, as a result of the piston approximation, we only encounter plane wave modes inside the cavity. We will subsequently omit the subscripts “00” for these coefficients. From the above linear equations, they are given in terms of the total membrane displacement as

$$A = -\frac{\rho\omega^2}{2k \sin kL} \left(u_0^{\text{ave}} \mathrm{e}^{-ikL} + u_L^{\text{ave}} \right), \tag{63}$$

$$B = -\frac{\rho\omega^2}{2k \sin kL} \left(u_0^{\text{ave}} \mathrm{e}^{ikL} + u_L^{\text{ave}} \right). \tag{64}$$

We have also directly substituted $\zeta_{00} = k$ and simplified the expression for L_{00} in the above expressions. These coefficients can now be substituted in place of the pressure into the right-hand side of (51) so as to give

$$\begin{aligned} &\sum_{m=0}^{\infty} \sum_{n=1}^{\infty} \rho_M d_M \Omega_{\text{mn}} C_{\text{mn}}^{0/L} u_{\text{mn}}(r, \phi) \\ &\quad = p_{0/L} + \frac{\rho\omega^2}{k} \left(u_{0/L}^{\text{ave}} \cot kL + u_{0/L}^{\text{ave}} \csc kL \right). \end{aligned} \tag{65}$$

The time component $\exp(i\omega t)$ cancels on both sides of the equation. We note that the right-hand side of the above equation system is independent of the spatial (r, ϕ) coordinates.

The above coupled system of equations can be considerably simplified by taking their sum and difference to obtain a new set of decoupled equations. After some algebra, we have the following set of “sum and difference” equations,

$$\sum_{m=0}^{\infty} \sum_{n=1}^{\infty} \rho_M d_M \Omega_{\text{mn}} C_{\text{mn}}^{+} u_{\text{mn}}(r, \phi) = p_+ + \frac{\rho\omega^2}{k} u_+^{\text{ave}} \cot \frac{kL}{2} \tag{66}$$

$$\sum_{m=0}^{\infty} \sum_{n=1}^{\infty} \rho_M d_M \Omega_{\text{mn}} C_{\text{mn}}^{-} u_{\text{mn}}(r, \phi) = p_- - \frac{\rho\omega^2}{k} u_-^{\text{ave}} \tan \frac{kL}{2} \tag{67}$$

where the “+” and “−” have been defined as the sum and difference of the respective “0/L” components. That is,

$$C_{\text{mn}}^{+} = C_{\text{mn}}^{L} + C_{\text{mn}}^{0}, \quad p_+ = p_L + p_0, \tag{68}$$

$$C_{\text{mn}}^{-} = C_{\text{mn}}^{L} - C_{\text{mn}}^{0}, \quad p_- = p_L - p_0, \tag{69}$$

$$u_+^{\text{ave}} = u_L^{\text{ave}} + u_0^{\text{ave}} = \sum_{m=0}^{\infty} \sum_{n=1}^{\infty} C_{\text{mn}}^{+} u_{\text{mn}}(r, \phi), \tag{70}$$

$$u_-^{\text{ave}} = u_L^{\text{ave}} - u_0^{\text{ave}} = \sum_{m=0}^{\infty} \sum_{n=1}^{\infty} C_{\text{mn}}^{-} u_{\text{mn}}(r, \phi). \tag{71}$$

Thus, it is apparent that the above system of equations is decoupled because the $u_{\pm}^{\text{ave}}$ terms can be expressed as a linear expansion of the respective $C_{\text{mn}}^{\pm}$ coefficients alone. Analogously to the calculation of the coefficients for the quasi-steady-state vibration in (46) and (48), we can now use the orthogonality of the membrane modes u_{mn} to determine the coefficients of the sum and difference vibrations in terms of the pressure and average membrane displacement,

$$C_{\text{mn}}^{+} \int \mathrm{d}S\, u_{\text{mn}} = \left[p_+ + \frac{\rho\omega^2}{k} u_+^{\text{ave}} \cot \frac{kL}{2} \right] \frac{K_{\text{mn}}}{\Omega_{\text{mn}}} \tag{72}$$

$$C_{\text{mn}}^{-} \int \mathrm{d}S\, u_{\text{mn}} = \left[p_- - \frac{\rho\omega^2}{k} u_-^{\text{ave}} \tan \frac{kL}{2} \right] \frac{K_{\text{mn}}}{\Omega_{\text{mn}}} \tag{73}$$

where

$$K_{\text{mn}} = \frac{\left(\int \mathrm{d}S\, u_{\text{mn}} \right)^2}{\rho_M d_M \int \mathrm{d}S\, u_{\text{mn}}^2}. \tag{74}$$

The integrals are over the vibrating part of the membrane surface S_{mem}. The substitution K_{mn} will simplify our calculations in the appendix for the estimation of membrane parameters. The next step will be to sum both sides of (72) and (73) over all the membrane eigenmodes (m, n). The left-hand sides of the equations give us

$$\sum_{m=0}^{\infty} \sum_{n=1}^{\infty} C_{\text{mn}}^{\pm} \int \mathrm{d}S\, u_{\text{mn}} = \pi a_{\text{cyl}}^2 u_{\pm}^{\text{ave}}. \tag{75}$$

Hence, we obtain exact expressions for the average membrane displacements,

$$\pi a_{\text{cyl}}^2 u_{\pm}^{\text{ave}} = \frac{p_L \pm p_0}{1 + \Lambda_{\text{tot}} \Gamma_{\pm}}. \tag{76}$$

We have thus shown how the quantities Λ and $\Gamma_{\pm}$ first defined in (5), (6) and (7) emerge from our analysis. As stated earlier, the $\Gamma_{\pm}$ terms contain the effect of the coupling through the air cavity and Λ is the frequency response of the membrane to a pure tone of angular frequency ω. Qualitatively, we can see that the information about the membrane $(a_{\text{tymp}}, c_M, \alpha)$ is contained within Λ, whereas the properties of the internal cavity $(V_{\text{cav}}, a_{\text{cyl}}, L)$ are contained in $\Gamma_{\pm}$. That is, we have obtained the results first motivated in (5)–(7),

$$\Lambda = \sum_{m,n}^{\infty} \frac{u_{\mathrm{mn}}(r,\phi) \int u_{\mathrm{mn}}}{\rho_M d_M \Omega_{\mathrm{mn}} \int u_{\mathrm{mn}}^2}, \quad \Lambda_{\mathrm{tot}} = \int_{S_{\mathrm{mem}}} \Lambda(r,\phi) \mathrm{d}S, \tag{77}$$

$$\Gamma_+ = -\frac{\rho c^2}{V_{\mathrm{cav}}} kL \cot kL/2, \quad \Gamma_- = \frac{\rho c^2}{V_{\mathrm{cav}}} kL \tan kL/2. \tag{78}$$

Subsituting the above expressions along with (76) into (72) and (73) gives us the results mentioned at the start of this section,

$$u_{0/L}(r,\phi) = \frac{1}{2}\left(\frac{p_L + p_0}{1 + \Lambda_{\mathrm{tot}}\Gamma_+} \mp \frac{p_L - p_0}{1 + \Lambda_{\mathrm{tot}}\Gamma_-}\right)\Lambda(r,\phi) \tag{79}$$

3.3.2 *Convergence of* Λ

Since the membrane frequency response $\Lambda(r,\phi)$, or equivalently Λ_{tot} in (77), is the summation of an infinite number of eigenmodes, in order to proceed with a numerical analysis of our model we first need to ensure that it converges to a finite value. Through the Cauchy–Schwarz inequality, we obtain

$$|\Lambda_{\mathrm{tot}}| \leq \mathscr{S}_{\mathrm{tymp}} \sum_{m,n} K_{\mathrm{mn}}/|\rho_M d_M \Omega_{m,n}| < \infty \tag{80}$$

with $\mathscr{S}_{\mathrm{tymp}}$ as the tympanic area and K_{mn} as the coefficient defined in (74). The former inequality is Cauchy–Schwarz, the latter is a general characteristic of the spectrum of the two-dimensional Laplacian associated with the eardrum; cf. (30), (47), and Table 1. We now need to approximate Λ_{tot} by choosing an appropriate mode cutoff based on the hearing range of the animal and the high damping at their corresponding eigenfrequencies. In our analysis, we chose a cutoff of $N = 30$ modes. The basic method involves arranging the modes in increasing order of eigenfrequency (or equivalently μ_{mn}). As a result, we can express the summation over a single index. In general, for the frequency ranges of the animals we are interested in, we need not calculate the summation beyond the first 30 eigenmodes. The damping at these frequencies sufficiently suppresses higher modes with respect to the lower ones.

Before we compare our model with experimental data, we take a look at the frequency dependence of individual membrane vibrations in Fig. 12a, b. In both cases, the real part $\Re\{\Lambda_{\mathrm{tot}}\}$ has a low-pass response, i.e., it is more or less frequency independent up to the membrane eigenfrequency f_0 and sharply drops to zero afterward. The imaginary part $\Im\{\Lambda_{\mathrm{tot}}\}$, on the other hand, has a band-pass response where it peaks close to, but beyond $f = f_0$ and falls off thereafter. The properties of $\Re\{\Lambda_{\mathrm{tot}}\}$ and $\Im\{\Lambda_{\mathrm{tot}}\}$ will be used to estimate membrane parameters in "Appendix" section. Moreover, as we will see in the next section, the behavior of the hearing cues (time and level differences) mirrors that of the membrane response.

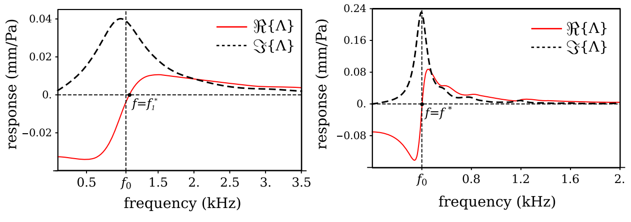

(a) **(b)**

Fig. 12 Real ($\Re$) and imaginary ($\Im$) part of the membrane frequency response for the ICE Model description of **a** Gecko and **b** *Varanus*. In both cases, the response is dominated by the fundamental frequency of the tympanic membrane. The presence of local maxima in the response of Varanus is a result of its comparatively low membrane damping. The frequency at which the response becomes purely imaginary is denoted by f_* and will be discussed in more detail in Sect. 4.5. Compare with Figs. 17 and 18

Table 2 Sysem parameters

Parameter	Gecko	Varanus
Interaural distance L	22 mm	16 mm
Eardrum radius a_{tymp}	2.6 mm	2.6 mm
Membrane density ρ_M	1 mg/mm^3	1.2 mg/mm^3
Eardrum thickness d_M	10 μm	30 μm
Cavity volume V_{cav}	3.5 ml	2.0 ml
Cylinder radius a_{cav}	6.6 mm	6.3 mm
Fundamental frequency f_0	1.05 kHz	0.4 kHz
Damping coefficient α	$\approx$2611 s^{-1}	$\approx$350 s^{-1}

4 Comparison with experiments

With the expressions derived in (79), we can compare our ICE model with experimental results. Using parameters based on standard anatomical data (see Table 2) and an extracolumellar angle $\beta = \pi/30\,(=6°)$, we get a membrane vibration velocity of $c_M = 5.4$ m/s for the *T. gecko* (*Gecko*) and $c_M = 2.9$ m/s for the water monitor (*Varanus*). This difference in c_M/f_0 also results in considerable differences in the nature of their hearing cues. Nevertheless, the ICE model adequately explains the generation of hearing cues in both species. In our subsequent computations, we take the speed of sound in air to be $c = 343\,\mathrm{ms}^{-1}$ and the density of air as $\rho = 1.206\,\mathrm{kgm}^{-3}$.

4.1 Interaural transmission gain

In the earlier literature (Christensen-Dalsgaard and Manley 2008; Christensen-Dalsgaard et al. 2011) on hearing in animals with internally coupled ears, the effect of interaural coupling on eardrum vibration was quantified by means of the so-called interaural transmission gain. This is defined as the response ratio of eardrum vibrations to unilateral local stimulation. In other words, calculating the ratio of the responses of both eardrums to an external stimulus presented to a single eardrum by using, for example, a closely placed headphone, with the contralateral ear effectively receiving *no* external input. The contralateral eardrum is therefore driven solely by the internal pressure setup by the vibrations of the ipsilateral one. A better understanding of ICE could nevertheless be gained by instead studying the responses of both eardrums to simultaneous and, therefore, realistic inputs separated by a small direction-dependent time difference.

Without loss of generality, we can mathematically derive the transmission gain G_T by setting $p_0 = 0$ and $p_L = p\exp(i\omega t)$ in (79). The resulting ipsi- and contralateral eardrum vibration amplitudes are then used to calculate G_T,

$$u_{0/L}(r,\phi) = \frac{1}{2}\left(\frac{p\exp(i\omega t)}{1+\Lambda_{\text{tot}}\Gamma_+} \mp \frac{p\exp(i\omega t)}{1+\Lambda_{\text{tot}}\Gamma_-}\right)\Lambda(r,\phi).$$

$$\Rightarrow G_T^{-1} = \left(\frac{u_0}{u_L}\right)^{-1} = \cos kL + \frac{V_{\text{cav}}\sin kL}{\rho c^2 \Lambda_{\text{tot}} kL}. \tag{81}$$

The mathematical expressions (78) for $\Gamma_\pm$ allow us to reach the considerably simplified formula (81).

In Fig. 13a, b, the values of the phase and amplitude of the transmission gain calculated through ICE have been plotted together with the experimentally determined values for (a) *Hemidactylus frenatus*, the common house gecko, and (b) the *T. gecko*. There is a fair agreement between calculated and experimental values.

The minor discrepancy in Fig. 13b for *Tokay* can be explained using the fact that there was a large size and hence weight variation (24–70 g) among the experimental specimens (Christensen-Dalsgaard et al. 2011). Variations in size lead to similar variations in the membrane fundamental frequency and can lead to considerable changes in the frequency behavior of the system. In the following sections, we will see examples of this variation across two species when we compare the frequency behavior for an adult gecko with that of a juvenile varanus.

4.2 Decibel vibration velocity: v_{dB}

In order to compare our model with experimental results, we define the average vibration velocity in dB re mms^{-1} Pa^{-1}, meaning the decibel velocity with respect to 1 mm/s for an input pressure amplitude of 1 Pa as $v_{\text{dB}} = 20\log_{10}|\dot{u}^{\text{ave}}_{0/L}|$. Fig. 14a, b show the respective frequency dependence of the membrane vibrations for ipsilateral $\theta = 90°$ and contralateral $\theta = -90°$ stimuli for both *Gecko* and *Varanus*.

In the case of *Gecko*, the contralateral response has a minimum near f_0, whereas the spectral response of *Varanus* shows multiple peaks corresponding to higher membrane eigenfrequencies. The occurrence of multiple peaks instead of a single one in the biophysically relevant range of up to 2 kHz is due to the fact that the eardrum of *Varanus* is very underdamped [much smaller α; cf. (30)], resulting in higher modes being less suppressed. Nevertheless, the present ICE model explains the frequency behavior in both cases and allows for a determination of the tympanic fundamental frequency in the alive animal; see the Appendix.

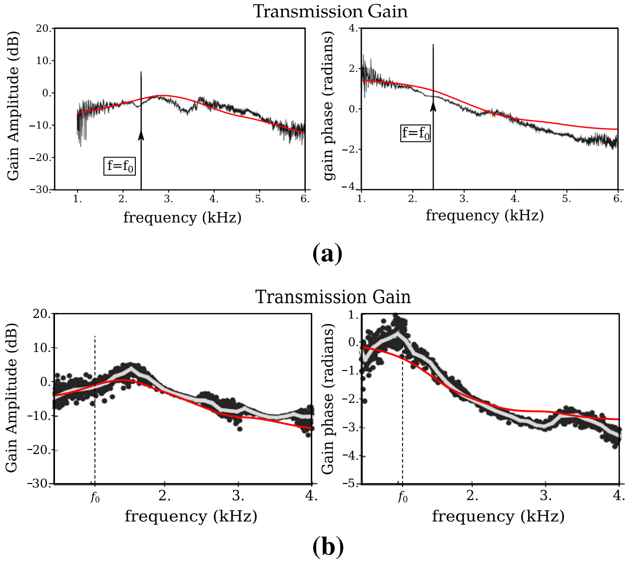

Fig. 13 **a** experimental and calculated transmission gain for *Hemidactylus* (common house gecko). The transmission gain G_T is defined as the response ratio of contra- and ipsilateral eardrum vibrations under unilateral stimulation; see (81). The *black lines* correspond to values experimentally determined by Christensen-Dalsgaard and Manley (2008) and the smooth *solid* (*red*) lines to values calculated to the ICE model. *Left* amplitude in decibels and *right* phase in radians. **b** experimental and calculated values of transmission gain for *Tokay*. The values were experimentally measured by Christensen-Dalsgaard et al. (2011) for five lightly anesthetized specimens. All the presented experimental data have been gathered through laser Doppler vibrometry measurements on the membrane surface. *Left* amplitude in decibels and *right* phase in radians

Figure 15a, b show the variation of the membrane vibration velocity with direction for different frequencies in *Tokay* and *Varanus*, respectively. For both animals, the ipsilateral ear is on the right-hand side and corresponds to positive values for the angle in degrees with respect to the rostral-caudal axis. In both cases, the eardrum has a markedly higher vibration velocity for sounds coming from an ipsilateral than from a contralateral direction.

4.3 Membrane vibration pattern

The measured vibration patterns (Manley 1972a) are shown on the left in Fig. 16. The amplitudes were measured for eight locations on the membrane to find the pattern seen in the figure. At around 4 kHz, the vibration pattern distinctly

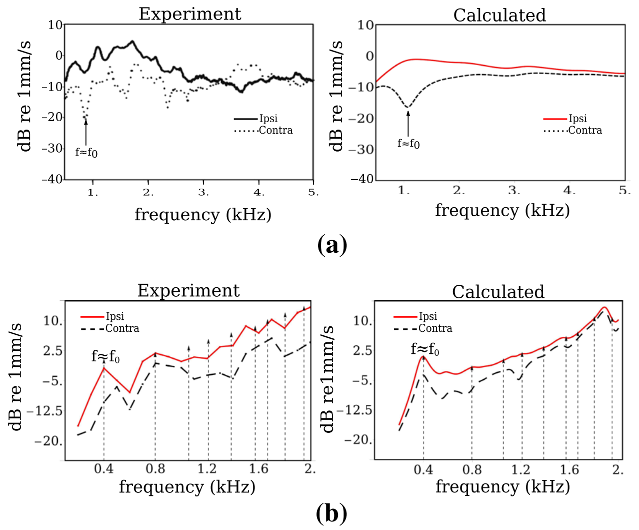

Fig. 14 *Top* experimental and calculated v_{dB} for ipsi- ($\theta = 90°$) and contralateral ($\theta = -90°$) stimuli for *Gecko*. *Bottom* experimental and calculated membrane amplitude for *Varanus* at $\theta = \pm 90°$. The vertical *dashed lines* in the lower plots correspond to the higher membrane modes for the Varanus. We thus see that not only at f_0 but also at higher membrane resonances does a less taut membrane with low α give peaks; compare Fig. 18b. The first resonant peak (or trough) allows a straightforward mathematical specification of the first extremum (max/min) for the iLD or equivalently the tympanic eigenfrequency f_0 in the alive animal. All experimental data presented were gathered through laser Doppler vibrometry. **a** Gecko. **b** Varanus

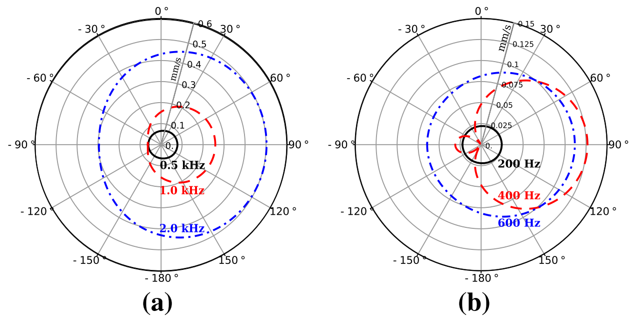

Fig. 15 Polar plots for the membrane vibration velocity in mm s^{-1} for different frequencies for **a** *Gecko* and **b** *Varanus*. Positive angles correspond to ipsilateral directions and negative angles to contralateral ones. The directionality of the system is immediately apparent from the way in which ipsilateral directions result in higher vibration amplitudes, even though the external inputs to the ears have the same amplitude. The above plots have been generated using the expression given in (79) using the parameters from Table 2. The input sound pressures have been assumed to have an amplitude of 60 dB SPL

develops two maxima—something that would not happen to a centrally loaded tympanum except at frequencies well beyond the hearing range of Geckos (200 Hz–3 kHz).

In order to compare our ICE model with the experimental results, we now plot the response of one of the membranes to an ipsilateral stimulus. This is calculated by using (79) and is illustrated in Fig. 16 (right) for the same frequency range as that of the experimental data.

The asymmetric nature of our membrane vibration pattern is a result of the chosen geometry. Mathematically, it is a result of the fact that a uniform pressure on the surface of a full circular membrane only couples to the circularly symmetric J_0 modes. The extracolumella, however, breaks this symmetry and all the resulting eigenmodes couple with the pressure, which offers a clear contrast to Fig. 9. As qualitative and semiquantitative reproduction, the present model is very strong, but for a full quantitative analysis, we would need to take into account both the microstructure of the tympanum and the motion of the extracolumella.

4.4 Internal time and level differences

Although the membrane vibration amplitudes are directional by themselves, the difference between left and right tympanum is more sensitive to the source direction θ. In the following, we focus on three universal aspects of ICE:

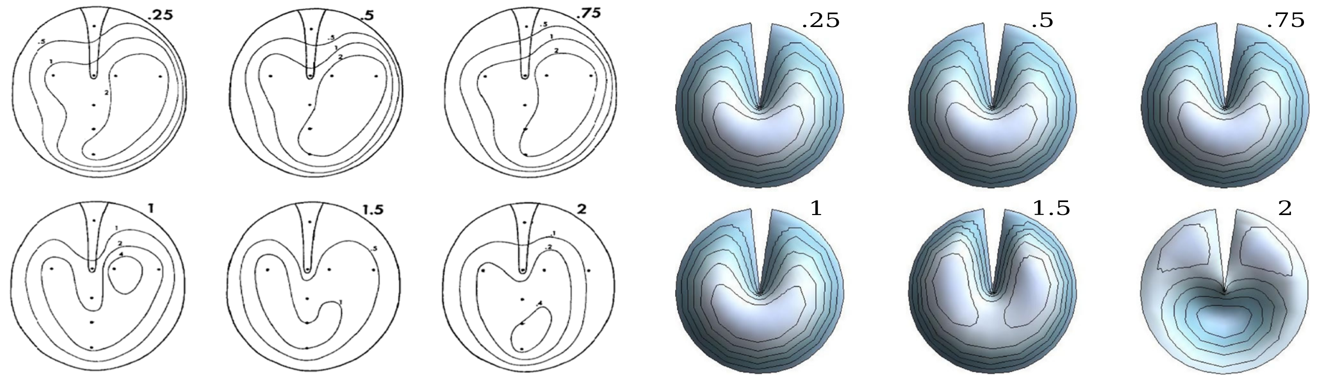

Fig. 16 *Left* experimental membrane vibration patterns of the *T. gecko* dependent on sound frequency varying from 0.25 to 2 kHz, with the corresponding frequencies shown above the membranes (Manley 1972a). *Right* vibration pattern of one of the membranes in the ICE model for an ipsilateral stimulus. In both cases, we see a similar complex vibrational pattern for the membranes, which becomes increasingly circularly asymmetric with increasing frequency

1. the internal time difference (**i**TD), which for frequencies $< f_0$ greatly exceeds the interaural time difference (**I**TD) and forms a plateau from $f = 0$ onwards;
2. the internal level difference (**i**LD), which exhibits a pronounced maximum once the iTD has strongly decreased; and
3. the fundamental frequency f_0 of the tympanum segregating the iTD and iLD domain.

Both iTD and iLD also depend on the sound-source direction. Moreover, the directionality of the hearing cues experienced by the animal directly reflect the nature of the stimulus. Finally, it should be constantly borne in mind that what the animal actually "hears" is not the interaural but the internal stimulus. These two may greatly differ.

The internal time difference (iTD) corresponds to the actual time difference between left and right membrane vibrations as experienced by the animal,

$$\text{iTD} = \text{Arg}\left(\dot{u}_L^{\text{ave}}/\dot{u}_0^{\text{ave}}\right)/\omega = \text{Arg}\left(u_L^{\text{ave}}/u_0^{\text{ave}}\right)/\omega, \tag{82}$$

$$u_L^{\text{ave}}/u_0^{\text{ave}} = (1+B)/(1-B) \tag{83}$$

where

$$B = i\,\left[(1+\Lambda_{\text{tot}}\Gamma_+)\,/\,(1+\Lambda_{\text{tot}}\Gamma_-)\right]\tan(k\Delta/2) \tag{84}$$

is direction-dependent through $\Delta = L\sin\theta$. The expression can be easily derived using the expressions for u_0^{ave} and u_L^{ave} in (79),

$$\begin{aligned}\frac{u_L^{\text{ave}}}{u_0^{\text{ave}}} &= \frac{p_+(1+\Lambda_{\text{tot}}\Gamma_-)+p_-(1+\Lambda_{\text{tot}}\Gamma_+)}{p_+(1+\Lambda_{\text{tot}}\Gamma_-)-p_-(1+\Lambda_{\text{tot}}\Gamma_+)}\\ &= \frac{1+\frac{p_-}{p_+}(1+\Lambda_{\text{tot}}\Gamma_+)/(1+\Lambda_{\text{tot}}\Gamma_-)}{1-\frac{p_-}{p_+}(1+\Lambda_{\text{tot}}\Gamma_+)/(1+\Lambda_{\text{tot}}\Gamma_-)}\\ &= \frac{1+i\tan(k\Delta/2)(1+\Lambda_{\text{tot}}\Gamma_+)/(1+\Lambda_{\text{tot}}\Gamma_-)}{1-i\tan(k\Delta/2)(1+\Lambda_{\text{tot}}\Gamma_+)/(1+\Lambda_{\text{tot}}\Gamma_-)}.\end{aligned} \tag{85}$$

The last step follows from the fact that

$$\begin{aligned}p_+ = p_L + p_0 &= p\,(\exp(ik\Delta/2)+\exp(-ik\Delta/2))\\ &= 2p\cos k\Delta/2,\\ p_- = p_L - p_0 &= p\,(\exp(ik\Delta/2)-\exp(-ik\Delta/2))\\ &= 2ip\sin k\Delta/2.\end{aligned}$$

The interaural time difference (ITD) for a given sound input (2) is $\text{Arg}\,(p_0/p_L)\,/\omega = L\sin\theta/c$, viz., the time difference between the arrival of sound from a given source at both ears. It is independent of frequency, and for our parameters, it is $\approx$64 µs for $\theta = \pm 90°$ for *Gecko* and $\approx$45 µs for a young *Varanus*. Figure 17a, b show the frequency and direction dependence of the internal time difference (**i**TD) for *Gecko* and *Varanus*, respectively. Experimentally, by measuring the phase difference between the eardrum vibrations, one in fact measures the iTD.

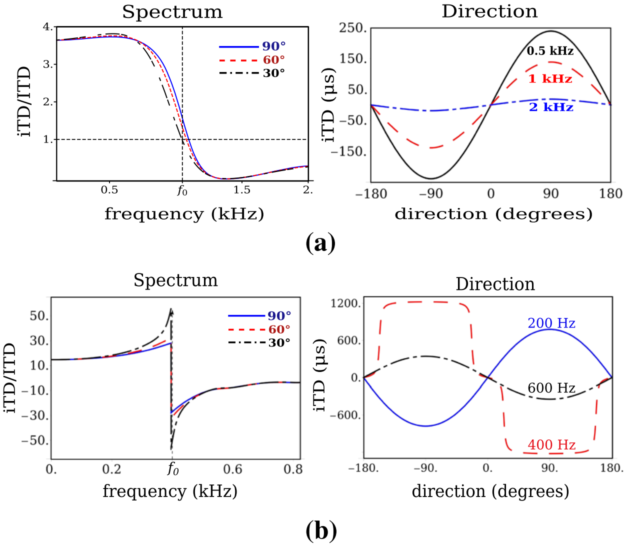

Fig. 17 Frequency and direction dependence of the iTDs for **a** *Gecko* (top) and **b** *Varanus* (bottom). **a** For *Gecko*, the iTDs exhibit a plateau of iTD $\approx$ 3.5 ITD, up to about $f = f_0$ and sharply fall thereafter. As indicated, the plateau is uniform, irrespective of the direction θ. Due to the plateau, the iTDs can thus be effective low-frequency cues. **b** For *Varanus*, the iTDs slowly increase up to f_0 and then decrease; the discontinuity is an artifact of 2π which corresponds to a loss of directional information in the iTD. The young animal can therefore only exploit a restricted low-frequency range of iTDs (up to approximately 200 Hz), nevertheless, illustrating that the time expansion factor iTD/ITD can differ from 3 appreciably

In the case of *Gecko*, the iTDs have a low-pass response, i.e., they are more or less constant up to a certain frequency and drop sharply thereafter, with iTD/ITD $= 1$ at $f \approx f_0$. From a neuronal-processing point of view, this is convenient as it mirrors the behavior of the ITDs, *but strongly increased* by a factor of about 3.5 for $0 \le f \lesssim \frac{2}{3} f_0$ in *Gecko* and an astounding 15 for $0 \le f \lesssim 0.2 f_0$ in *Varanus*; cf. Fig. 17a, b (left). The number 3.5 depends on the specific geometry of the internal cavity as found in many lizards, such as *Gecko*, but it is not unique. Figure 17b illustrates its variation for *Varanus*.

For the input (2), the internal Level Difference (iLD) is defined as the logarithmic difference between the left and right (0/L) membrane amplitudes of (46), i.e.,

$$\text{iLD} = 20\,\text{Log}_{10}|u_L^{\text{ave}}/u_0^{\text{ave}}| = 20\,\text{Log}_{10}|\dot{u}_L^{\text{ave}}/\dot{u}_0^{\text{ave}}|, \tag{86}$$

Once left and right inputs effectively have the same amplitude, we can put the interaural level difference (ILD) equal to zero. For *Gecko*, the iLD has a band-pass like behavior.

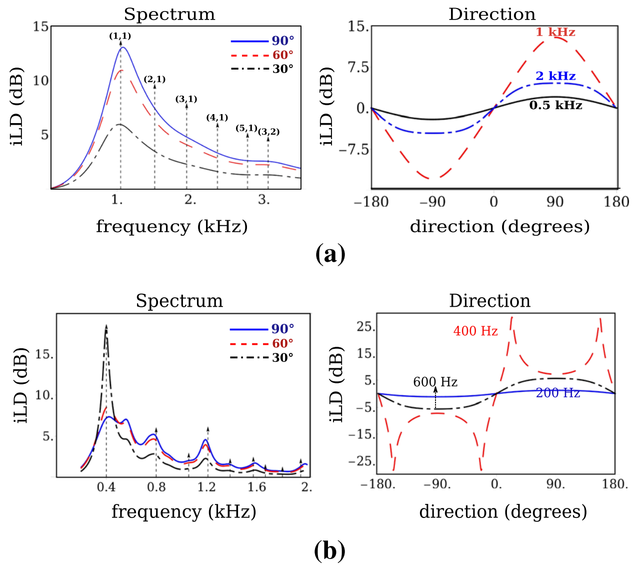

Fig. 18 Calculated frequency and direction dependence of the iLDs for **a** *Gecko* (*top*) and **b** *Varanus* (*bottom*). The location of the eigenfrequencies has been indicated by *dashed arrows*. For *Gecko*, the iLDs peak close to $f = f_0$ and decrease slowly thereafter. They can therefore serve both as effective high-frequency hearing cues and as an efficient means of determining f_0 in alive animals. Clearly, the higher tympanic eigenmodes play no role. For juvenile *Varanus* with small α and $f_0 \approx 500$ Hz, we see the corresponding peaks of some (at least five) higher membrane eigenmodes

It is zero for both very low and high frequencies and peaks close to the membrane eigenfrequency f_0; cf. Fig. 18a. The iLDs steeply increase across $\theta = 0°$ and attain a maximum/minimum at $\theta = \pm 90°$. Under normal circumstances, as in *Gecko*, the functional dependence is given by a sine. For *Varanus*, Fig. 18b shows an iLD spectrum with multiple peaks near membrane resonances (i.e., eigenfrequencies), corresponding to a much lower damping (smaller α). Moreover, at the fundamental membrane eigenfrequency f_0, the directional response peaks at $\theta = \pm 30°$. A possible explanation of this deviating behavior is that the experiments were performed on juvenile monitor lizards, suggesting that increased membrane damping and cavity volume in adults should give similar results to those shown for the adult *Gecko*.

4.5 Role of the membrane response function Λ

A parallel between the frequency response of the internal time and level differences (iTD and iLD), and the membrane frequency response $\Lambda(r, \phi)$ (5) should be immediately apparent; compare Figs. 12, 17 and 18. This similarity results from the way in which we have defined the ratio of the complex vibration amplitudes (83), (84). Furthermore, it explains the role of the membrane eigenfrequency in the generation of interaural cues. Using our definition of B (83), the ratio between the membrane vibration amplitudes can therefore be rewritten as,

$$u_L^{\text{ave}}/u_0^{\text{ave}} = \frac{\exp(ik\Delta/2) + \Lambda_{\text{tot}}(\Gamma_- \cos\frac{k\Delta}{2} + i\Gamma_+ \sin\frac{k\Delta}{2})}{\exp(-ik\Delta/2) + \Lambda_{\text{tot}}(\Gamma_- \cos\frac{k\Delta}{2} - i\Gamma_+ \sin\frac{k\Delta}{2})}.$$

We now focus on the case where the sound source is at $\theta = \pi/2 (= 90°)$ and, subsequently, $\Delta = L$. This means that the sound source is on the same side as the L ear; cf. Fig. 7. The ratio between the membrane vibrations can therefore be explicitly written down

$$\begin{aligned} u_L^{\text{ave}}/u_0^{\text{ave}} &= \frac{\exp(ikL/2) + \tilde{\Lambda}_{\text{tot}}(\sin kL/2 - i\cos kL/2)}{\exp(-ikL/2) + \tilde{\Lambda}_{\text{tot}}(\sin kL/2 + i\cos kL/2)}, \\ &= \frac{\exp(ikL/2) - i\tilde{\Lambda}_{\text{tot}}\exp(ikL/2)}{\exp(-ikL/2) + i\tilde{\Lambda}_{\text{tot}}\exp(-ikL/2)}, \\ &= \exp(ikL)\frac{1 - i\tilde{\Lambda}_{\text{tot}}}{1 + i\tilde{\Lambda}_{\text{tot}}}. \end{aligned} \tag{87}$$

We have used the definitions of $\Gamma_\pm$ from (78) and absorbed the factor $\rho c^2 kL/V_{\text{cav}}$ into Λ_{tot} by defining

$$\tilde{\Lambda}_{\text{tot}} = \rho c^2 kL\Lambda_{\text{tot}}/V_{\text{cav}}. \tag{88}$$

From Fig. 12a, b, we can see that there is a frequency f_* where the membrane response becomes purely imaginary. Let us assume that at this point, $\tilde{\Lambda}_{\text{tot}} = i\eta$ where η is a positive real number which carries information about both the tympanic membrane as well as the internal cavity. The ratio (87) reduces to

$$u_L^{\text{ave}}/u_0^{\text{ave}} = \exp(ikL)\frac{1 + \eta}{1 - \eta}. \tag{89}$$

The right-hand side of the above equation is a phase factor multiplied by a real number. The argument of the quantity kL is equal to the phase difference between the inputs to the eardrums and, due to our definition of iTD (82), the resultant internal time difference between the ears *equals* the interaural time difference. The corresponding values for f_* can be calculated numerically and are found to be around 1097 Hz for *Gecko* and around 402 Hz for *Varanus*.

For directions other than $\theta = 90°$, a similar result can be obtained, but the exact value of f_* in this case would also depend on the cavity volume. It is only when the source is fully ipsilateral/contralateral to an ear, that f_* can be determined solely from the membrane parameters.

4.6 iTD/iLD transition

From the low-pass behavior of the iTDs and the high-pass behavior of the iLDs, we can infer that internal time differences may well work as effective cues at lower frequencies,

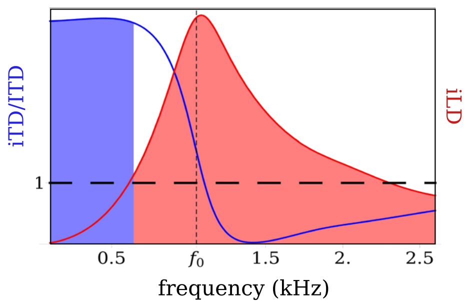

Fig. 19 Transition between the iTD and iLD frequency regimes for directions $\theta \neq 0°$. At lower frequencies, iTDs work better as directional cues, e.g., with iTD/ITD ≈ 3 for adult lizards, while at higher frequencies, the iLDs become pronounced, even though for most lizards, the external $ILD \approx 0$. The transition between the two kinds of cues is governed by the eardrum's fundamental eigenfrequency f_0

whereas internal level differences are most effective at higher frequencies. Unlike larger animals where such a transition would rely on the fact that higher-frequency sound waves would have a "shadow" on the contralateral eardrum due to diffraction (p. .154 Fletcher 1992), the iTDs and iLDs in ICE are generated solely as a consequence of the internal coupling between the eardrums.

In animals with ICE, the transition between the different frequency regimes is governed by the fundamental frequency of the tympanic membrane; see Fig. 19. Despite the lack of an amplitude difference between the inputs, the system uses small phase differences to generate frequency-dependent time (or equivalently phase) and amplitude differences between the eardrums by using the internal coupling and the mechanics of the membrane.

4.7 Volume dependence

In the ICE Model, the volume of the internal cavity is an independent parameter, which determines the strength of the internal coupling and in a mathematical analysis can be used at will. That is, to satisfy our scientific curiosity. In Fig. 20a, b, we see the frequency dependence of the iTDs and iLDs (at source direction $\theta = 90°$) for different cavity volumes while keeping the other system parameters fixed. The lower limit of possible cavity volumes is equal to that of a cylinder with a radius equal to that of the membrane, i.e., $a_{\text{cyl}} \geq a_{\text{tymp}}$, leading to a cross-sectional area of $\pi a_{\text{tymp}}^2 L$.

The volume dependence arises from the coupling parameters $\Gamma_\pm$ defined in (7) which decrease with the volume as $1/V_{\text{cav}}$. This means that as we let the volume go to infinity while keeping the interaural distance L constant ($a_{\text{cyl}} \to \infty$), the eardrums vibrate as uncoupled membranes driven by the sound pressures $p_{0/L}$

$$u_{0/L}(r, \phi; t) = \Lambda(r, \phi) p_{0/L}. \tag{90}$$

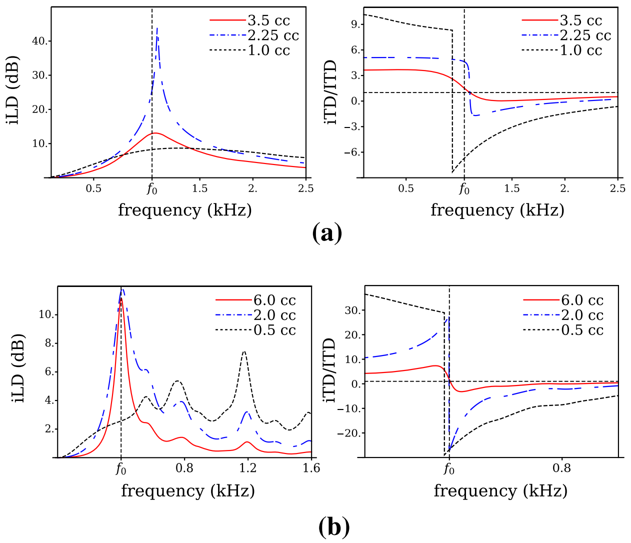

Fig. 20 iTD and iLD frequency response for different cavity volumes for **a** *Gecko* (top) and **b** *Varanus* (bottom). The sound source direction was chosen to be $\theta = 90°$. As we increase V_{cav}, the iLDs become smaller and less sharp around f_0. The iTDs on the other hand increase with decreasing volume, but also result in a phase ambiguity of 2π close to f_0. At an optimal volume of $\approx$2.2 cc for the *T. gecko* and 6 cc for *Varanus*, we have an optimal frequency response for both hearing cues

$\Lambda(r, \phi)$ essentially gives us the frequency response of the membrane amplitude at a given point (r, ϕ) on its surface.

For *Gekko* as well as for *Varanus*, the iLD goes to zero for small volumes. The iTD, on the other hand, appears to increase. However, it loses its plateau which is important for auditory information processing for low frequencies and develops a phase ambiguity of 2π close to f_0. This means that the eardrums vibrate with a phase difference of π and can no longer be used to localize sound sources. Thus, both very small and very large volumes effectively break the coupling between the membranes. For the *Tokay*, we find an optimal response, i.e., flat amplified iTDs at low frequencies and strong iLDs at higher frequencies for $V_{\text{cav}} \approx 2.2$ cc. This could be due to the fact that the assumed volume of 3.5 cc is for an "empty" skull. A live specimen would have a tongue and other organs inside the pharyngeal cavity which reduce the effective volume so that only the pharyngeal cavity remains.

Rather more interesting is the fact that for larger cavity volumes ($\approx$6 cc), the frequency response of the iLDs and iTDs of *Varanus* become similar to that of the *Gekko*; cf. Fig. 20b, solid (red) lines. The local iLD maxima corresponding to higher membrane modes are suppressed and the iTD has a fairly smooth and flat response at lower frequencies. This implies that the hearing system of an adult *Varanus* would me more effective at localizing sound sources, at least over a larger frequency range.

4.8 Critical volume

In Fig. 20a, b, we see that for a certain value of V_{cav}, a singularity appears for the iLD close to f_0 for a source direction $\theta = 90°$. A comprehension of what causes this singularity to emerge is essential to a complete understanding of ICE. The physical explanation for this apparent singularity is that at the critical volume, the internal pressure at the contralateral membrane cancels the external pressure at the frequency of maximal iLD response. As a result, the contralateral membrane vibration velocity, or equivalently the displacement, vanishes entirely, i.e., $u_0(r, \phi; t) = 0$. Hence, by definition, the iLD is bound to diverge.

This result can be derived directly from the expression for the membrane displacement (4). Rewriting u_0 explicitly in terms of input pressure amplitude and direction gives us

$$u_0(r, \phi) = \frac{1}{2}\left(\frac{2p\cos k\Delta/2}{1+\Lambda_{\mathrm{tot}}\Gamma_+} - \frac{2ip\sin k\Delta/2}{1+\Lambda_{\mathrm{tot}}\Gamma_-}\right)\Lambda(r, \phi).$$

For a sound source closer to the L ear, the opposite 0 ear is on the contralateral side; see Fig. 7. We thus have $\Delta = L\sin\theta = L$ for $\theta = \pi/2$ $(= 90°)$. The displacement can be rewritten as

$$u_0(r, \phi) = \left(\frac{p\cos kL/2}{1+\Lambda_{\mathrm{tot}}\Gamma_+} - \frac{ip\sin kL/2}{1+\Lambda_{\mathrm{tot}}\Gamma_-}\right)\Lambda(r, \phi)$$

where the $1/2$ has been absorbed into the brackets. As shown in Sect. 4.5, the frequency where $iTD = ITD$, viz., f_*, is achieved when the membrane frequency response Λ (5) becomes purely imaginary. As derived in (88) let us suppose that $\tilde{\Lambda}_{\mathrm{tot}}(f = f_*) = i\eta$, where η is a real number and consider the case where $V_{\mathrm{cav}} = \rho c^2 kL\eta$ so that the factor $\frac{\rho c^2 kL\eta}{V_{\mathrm{cav}}}$ in the denominators beside the tan and cos becomes equal to 1. Using the definitions of $\Gamma_\pm$ (7) at $f = f_*$, we find

$$\begin{aligned} u_0(r, \phi) &= \left(\frac{p\cos kL/2}{1-i\cot kL/2} - \frac{ip\sin kL/2}{1+i\tan kL/2}\right)\Lambda(r, \phi), \\ &= \left(\frac{ip\sin kL/2}{1+i\tan kL/2} - \frac{ip\sin kL/2}{1+i\tan kL/2}\right)\Lambda(r, \phi), \\ &= 0. \end{aligned}$$

In the second equation, we have multiplied and divided the first fraction by $i\tan kL/2$. It is thus clear that for this cavity volume, the membrane displacement on the contralateral side identically vanishes resulting in a singularity of the iLD, actually a trivial one. Nevertheless we can safely use the term "critical" to denote this cavity volume $V_{\mathrm{crit}} = \rho c^2 kL\eta$.

For the animal, V_{crit} is not an optimal cavity volume to fully exploit interaural coupling. This is mainly due to the fact that the iTD response starts to show a phase ambiguity on either side of f_*; cf. Fig. 20b (right). The animal would be unable to distinguish between sources on the left and the right and would therefore be better off by operating with a cavity volume slightly above V_{crit}, where a strong iLD is coupled with an unambiguous iTD response.

This is also a possible explanation of the deviations observed in the hearing cues for the juvenile *Varanus* when we compare it with *Gecko*. Given its other system parameters, i.e., membrane eigenfrequency, damping, interaural separation, the volume of 2.0 cc in *Varanus* is well below its V_{crit} of 6 cc.

5 Discussion

In this review, we have shown that by modeling the internal cavity as an air-filled cylinder, we can simultaneously calculate the quasi-steady-state vibration amplitudes of a pair of coupled membranes as well as the internal pressure driving them. Using these amplitudes, we were able to calculate hearing cues such as the *internal* time and level differences in (82) and (86). These are functions of direction and frequency and represent cues experienced by the animal.

The presence of the extracolumella has been accounted for by modeling the eardrum as a circular membrane with a non-moving sector of angle 2β; cf. Fig. 1c. As a result, we were able to reproduce the complex asymmetrical vibration patterns observed in live gecko specimens. In order, however, to exactly determine the vibration patterns observed in nature, we need to account for the microstructure of the tympanum and any associated inhomogeneities in its surface tension in the specific animal under consideration. This is outside the scope of the present review.

In the first biophysical model of ICE (Vossen et al. 2010; Vossen 2010), the volume of the cylinder was fixed by the interaural distance L and tympanic radius a_{tymp}. By instead allowing the volume of the cylinder to be a free parameter and using it to calculate the radius of the cylinder, we were able to analyze its effect on the coupling between the membranes in three different animal classes: frogs, lizards, and birds. Both very large and very small volumes effectively break the coupling between the membranes, albeit in different ways. Moreover, through a thorough analysis of the tympanic membrane, we were able to discern its relationship to the cavity volume in Sect. 4.8. This way, the animal could possibly "tune" its eardrum by varying its tension in order to optimize interaural coupling for a certain frequency range (Young et al. 2016).

With ICE, we have therefore come across a hearing system that relies on iTDs at low frequencies and iLDs at higher frequencies, with the transition between the two regimes being governed by the fundamental frequency f_0 of the tympanic membrane; see Fig. 19. In this way the fundamental frequency of the eardrum creates a partition of the sensory landscape.

Acknowledgments The authors gratefully acknowlege André Longtin's (uOttawa) constructive criticism. They also thank David Heider for an enjoyable collaboration on the mathematical foundations of the perturbation theory used here.

Appendix: Estimating the eardrum's fundamental frequency and damping coefficient

The fundamental frequency f_0 and the damping coefficient α of the eardrum are important quantities to auditory performance. The former to partitioning the auditory landscape, the latter to determining the duration of transient response of the tympanum. How, then, can we determine them in the practice of experiment?

To detemine both, we need two quantities from experimentally measured tympanic vibration and hearing cues. As we see from Figs. 17 and 18, the maximum of the iLD as well as the frequency f_* at which, for say sound-source directions $\theta = \pm 90°$, the internal iTD equals the external ITD are experimentally accessible and near f_0.

We can analytically estimate the location of the iLD maximum and determine f_* in terms of f_0 by using the properties of the membrane frequency response Λ or, more specifically, Λ's integral over the membrane surface Λ_{tot}; cf. (77). An experimental recipe follows at the end of this appendix. Λ_{tot} has been defined as

$$\Lambda_{\mathrm{tot}} = \int_{S_{\mathrm{mem}}} \mathrm{d}S\, \Lambda(r,\phi) = \sum_{m,n}^{\infty} K_{\mathrm{mn}}/\Omega_{\mathrm{mn}} \tag{91}$$

where

$$K_{\mathrm{mn}} = \frac{\left(\int u_{\mathrm{mn}}\right)^2}{\rho_M d_M \int u_{\mathrm{mn}}^2}, \quad \Omega_{\mathrm{mn}} = \left(\omega^2 - \omega_{\mathrm{mn}}^2 - 2i\alpha\omega\right). \tag{92}$$

We can now explicitly split Λ_{tot} into its real and imaginary parts,

$$\Re\{\Lambda_{\mathrm{tot}}\} = \sum_{m,n}^{\infty} K_{\mathrm{mn}} \left(\omega^2 - \omega_{\mathrm{mn}}^2\right) \Big/ \left[\left(\omega^2 - \omega_{\mathrm{mn}}^2\right)^2 + 4\alpha^2\omega^2\right], \tag{93}$$

$$\Im\{\Lambda_{\mathrm{tot}}\} = \sum_{m,n}^{\infty} K_{\mathrm{mn}} 2\alpha\omega \Big/ \left[\left(\omega^2 - \omega_{\mathrm{mn}}^2\right)^2 + 4\alpha^2\omega^2\right]. \tag{94}$$

$\Re\{\Lambda_{\mathrm{tot}}\}$ and $\Im\{\Lambda_{\mathrm{tot}}\}$ have been plotted for *Gekko* and *Varanus* in Fig. 12a, b, respectively. We see that for a certain frequency f_*, $\Re\{\Lambda_{\mathrm{tot}}\} = 0$. In Sect. 4.5 we have also shown that exactly at $f = f_*$ the internal time difference iTD becomes equal to the interaural time difference ITD. Furthermore, it is possible to measure the corresponding iLD at f_*. Using the definition (89) of the membrane vibration–amplitude ratio at f_* and recalling that $\rho c^2 k L \Lambda_{\mathrm{tot}}/V_{\mathrm{cav}}\big|_{f=f_*} = i\eta$, we obtain

$$\mathrm{iLD}\big|_{f=f_*} = 20\log_{10}\left|\frac{u_L^{\mathrm{ave}}}{u_0^{\mathrm{ave}}}\right| = 20\log_{10}\frac{1+\eta}{1-\eta}$$
$$\Rightarrow \eta = \frac{10^{\mathrm{iLD}/20} - 1}{10^{\mathrm{iLD}/20} + 1}. \tag{95}$$

Thus, by measuring the iLD at f_*, we can calculate the imaginary part of the membrane frequency response as well. We should also note here that η is a dimensionless quantity. The resulting *nonlinear* equations in α and ω_{mn} are given by

$$\Re\{\Lambda_{\mathrm{tot}}\}\big|_{f=f_*} = \sum_{m,n}^{\infty} \frac{K_{\mathrm{mn}}\left(\omega_*^2 - \omega_{\mathrm{mn}}^2\right)}{\left(\omega_*^2 - \omega_{\mathrm{mn}}^2\right)^2 + 4\alpha^2\omega_*^2} = 0 \tag{96}$$

$$\Im\{\Lambda_{\mathrm{tot}}\}\big|_{f=f_*} = \sum_{m,n}^{\infty} \frac{K_{\mathrm{mn}} 2\alpha\omega_*}{\left(\omega_*^2 - \omega_{\mathrm{mn}}^2\right)^2 + 4\alpha^2\omega_*^2} = \frac{\eta V_{\mathrm{cav}}}{\rho c L \omega_*} \tag{97}$$

where $\omega_* = 2\pi f_*$. We have also used the fact that $k = \omega/c$. Given the above equations, the problem boils down to calculing $f_0 = \omega_{11}/2\pi$ and α as the remaining eigenfrequencies are related to the fundamental eigenfrequency by $f_{\mathrm{mn}}/f_0 = \omega_{\mathrm{mn}}/\omega_{11} = \mu_{\mathrm{mn}}/\mu_{11}$. Here μ_{mn} is the nth zero of the Bessel function J_κ; cf. (39).

Having determined f_* as well as η through the corresponding iLD based on membrane vibration amplitudes, it would be possible to use (96) and (97) to obtain estimates for f_0 and α. This can be done by using standard iterative algorithms to find the roots of functions. A common example is the Newton–Raphson method (Ch. 5 Stoer and Bulirsch 2002). For a real-valued function f, in order to find an approximation for its roots $x : f(x) = 0$ we start with an initial guess of x_0. A better approximation for x is then given by

$$x_1 = x_0 - \frac{f(x_0)}{f'(x_0)}$$
$$x_{n+1} = x_n - \frac{f(x_n)}{f'(x_n)}.$$

To find a root for a system of two equations $(x, y) : g_1(x, y) = 0,\ g_2(x, y) = 0$ in two dimensions, we would instead need to calculate the appropriate Jacobian matrix,

$$\mathbb{J} = \begin{pmatrix} \frac{\partial g_1}{\partial x} & \frac{\partial g_1}{\partial y} \\ \frac{\partial g_2}{\partial x} & \frac{\partial g_2}{\partial y} \end{pmatrix}.$$

The corresponding iteration rule is given by

$$\begin{pmatrix} x_{n+1} \\ y_{n+1} \end{pmatrix} = \begin{pmatrix} x_n \\ y_n \end{pmatrix} - \mathbb{J}^{-1} \begin{pmatrix} g_1(x_n, y_n) \\ g_2(x_n, y_n) \end{pmatrix}. \tag{98}$$

In dimensions higher than 2, it is more feasible to multiply both sides of (98) by $\mathbb{J}$ and to solve the resulting system.

Since we only need to estimate two values, the inverse of the Jacobian can be easily calculated. The relevant variables for our numerical problem are $x = f_0$ and $y = \alpha$ and the corresponding equations are given by

$$g_1(f_0, \alpha) = \Re\{\Lambda_{\text{tot}}\}|_{f=f_*} = 0 \tag{99}$$

$$g_2(f_0, \alpha) = \Im\{\Lambda_{\text{tot}}\}|_{f=f_*} - \frac{\eta V_{\text{cav}}}{\rho c L \omega_*} = 0. \tag{100}$$

The derivatives needed to calculate the Jacobian are given by

$$\frac{\partial \Re\{\Lambda_{\text{tot}}\}}{\partial f_0} = \frac{2}{f_0} \sum_{m,n}^{\infty} \frac{K_{\text{mn}} \omega_{\text{mn}}^2 \left(\left(\omega_*^2 - \omega_{\text{mn}}^2 \right)^2 - 4\alpha^2 \omega_*^2 \right)}{\left| \Omega_{\text{mn}}^* \right|^4} \tag{101}$$

$$\frac{\partial \Re\{\Lambda_{\text{tot}}\}}{\partial \alpha} = 8\alpha\omega_*^2 \sum_{m,n}^{\infty} \frac{K_{\text{mn}} \left(\omega_*^2 - \omega_{\text{mn}}^2 \right)}{\left| \Omega_{\text{mn}}^* \right|^4}, \tag{102}$$

$$\frac{\partial \Im\{\Lambda_{\text{tot}}\}}{\partial f_0} = \frac{8\alpha\omega_*}{f_0} \sum_{m,n}^{\infty} \frac{K_{\text{mn}} \left(\omega_*^2 - \omega_{\text{mn}}^2 \right) \omega_{\text{mn}}^2}{\left| \Omega_{\text{mn}}^* \right|^4}, \tag{103}$$

$$\frac{\partial \Im\{\Lambda_{\text{tot}}\}}{\partial \alpha} = 2\omega_* \sum_{m,n}^{\infty} \frac{K_{\text{mn}} \left(\left(\omega_*^2 - \omega_{\text{mn}}^2 \right)^2 - 4\alpha^2 \omega_*^2 \right)}{\left| \Omega_{\text{mn}}^* \right|^4}. \tag{104}$$

where $\Omega_{\text{mn}}^* = \left(\omega_*^2 - \omega_{\text{mn}}^2 - 2i\alpha\omega_* \right)$. The Newton–Raphson method converges quadratically to the correct value of the root.

In order to simplify the estimation of the relevant parameters, it would be prudent to separate the dependence on the size of the membrane from terms that arise independently in the mathematical analysis. Specifically, we look at the coefficients K_{mn} as given by (92). Writing the integrals in the numerator and denominator explicitly we obtain

$$\int \mathrm{d}S\, u_{\text{mn}} = \int_{\beta}^{2\pi-\beta} \sin\kappa(\phi - \beta)\, \mathrm{d}\phi \int_0^{a_{\text{tymp}}} r J_\kappa\left(\mu_{\text{mn}} r\right)\, \mathrm{d}r$$

$$= \frac{1}{\kappa}\left[1 - \cos m\pi\right] \int_0^{a_{\text{tymp}}} r J_\kappa\left(\mu_{\text{mn}} r\right)\, \mathrm{d}r \tag{105}$$

and

$$= \frac{a_{\text{tymp}}^2}{\kappa}\left[1 - \cos m\pi\right] \int_0^1 \tilde{r} J_\kappa\left(a_{\text{tymp}} \mu_{\text{mn}} \tilde{r}\right)\, \mathrm{d}\tilde{r}$$

$$\int \mathrm{d}S\, u_{\text{mn}}^2 = \int_{\beta}^{2\pi-\beta} \sin^2\kappa(\phi - \beta)\, \mathrm{d}\phi \int_0^{a_{\text{tymp}}} r J_\kappa^2(\mu_{\text{mn}} r)\, \mathrm{d}r$$

$$= (\pi - \beta) \int_0^{a_{\text{tymp}}} r J_\kappa^2(\mu_{\text{mn}} r)\, \mathrm{d}r \tag{106}$$

$$= (\pi - \beta) a_{\text{tymp}}^2 \int_0^1 \tilde{r} J_\kappa^2\left(a_{\text{tymp}} \mu_{\text{mn}} \tilde{r}\right)\, \mathrm{d}\tilde{r}$$

where $\tilde{r} = r/a_{\text{tymp}}$. Recall that $a_{\text{tymp}} \times \mu_{\text{mn}}$ corresponds to the nth zero of J_κ. We have thus separated the geometrical parameter a_{tymp} from the Bessel integrals in (105) and (106). Furthermore, we see that the integral in (105) is nonzero (and equal to 2) only for odd values of m as $\cos m\pi = 1$ for even m.

Table 3 Numerical parameters needed for estimating f_0 and α

m	n	$\mu_{\text{mn}} \times a_{\text{tymp}}$	$\widetilde{K}_{\text{mn}}$
1	1	3.16602	0.3833
3	1	4.56064	0.04463
5	1	5.87051	0.01583
7	2	6.30889	0.02812
9	1	7.13348	7.822×10^{-3}
11	2	7.79759	4.13×10^{-4}
13	1	8.36586	4.56×10^{-3}
15	2	9.21062	5.666×10^{-8}
17	3	9.45094	0.03299
19	1	9.57637	2.938×10^{-3}
21	2	10.5742	3.541×10^{-5}
23	1	10.7703	2.026×10^{-3}
25	3	10.9788	4.775×10^{-3}
27	2	11.9022	6.028×10^{-5}
29	1	11.9512	1.467×10^{-3}
31	3	12.443	2.01×10^{-3}
33	4	12.5928	8.459×10^{-3}
35	1	13.1214	1.103×10^{-3}
37	2	13.2033	6.768×10^{-5}
39	3	13.8616	1.135×10^{-3}

For $\kappa[m] = 0.5\, m\pi/(\pi - \beta)$, $m = 1, 3, 5, \ldots$, we can rewrite K_{mn}

$$K_{\text{mn}} = \frac{16}{\pi^2} \frac{\mathscr{S}_{\text{tymp}}}{\rho_M d_M} \widetilde{K}_{\text{mn}},$$

$$\widetilde{K}_{\text{mn}} = \frac{\left(\int_0^1 \tilde{r} J_\kappa\left(a_{\text{tymp}} \mu_{\text{mn}} \tilde{r}\right)\, \mathrm{d}\tilde{r} \right)^2}{m^2 \int_0^1 \tilde{r} J_\kappa^2\left(a_{\text{tymp}} \mu_{\text{mn}} \tilde{r}\right)\, \mathrm{d}\tilde{r}}. \tag{107}$$

where $\mathscr{S}_{\text{tymp}} = (\pi - \beta) a_{\text{tymp}}^2$ is the surface area of the tympanum. The values of $\widetilde{K}_{\text{mn}}$ for 20 modes are given in Table 3 and are arranged in a descending order of $K_{\text{mn}}/\mu_{\text{mn}}^2$, which is the value of Λ_{tot} at $f = 0$. The $\widetilde{K}_{\text{mn}}$ are independent of the size of the membrane and depend only on the extracolumellar angle β.

Numerical calculations in experimental practice

In practice, we would need to choose an appropriate cutoff for the membrane eigenmodes. Ideally, we have to ensure that the last eigenmode has a frequency well above the hearing

Table 4 Estimated f_* and η

	Gekko	*Varanus*
f_* (Hz)	1097.78	402.664
η	0.666	1.697

range of the animal. In order to test our method for the numerical estimation of f_0 and α, we have started by performing simulations for *Gekko* and *Varanus* while using the first 70 membrane eigenmodes, with the 70th mode corresponding to an eigenfrequency of around 11.7 and 4.45 kHz for *Gekko* and *Varanus*, respectively;—well beyond the hearing range of either species. The estimated values of f_* and η are shown in Table 4. In a real-world experimental setup, these values would correspond to those estimated from measured membrane vibration amplitudes and phases.

We seek to test the accuracy of our method by assuming that the values calculated for 70 modes were obtained experimentally. In passing, "were" is meant to be a subjunctive. This way we can test the performance of the algorithm in case the experimenter only chooses a limited number of modes. To do so, we would first need initial guesses for f_0 and α. For the fundamental frequency we can take f_* itself as eyeballing the iTD plots tells us that the values are fairly close to each other; cf. Fig. 17a, b. Based on the behavior of the membrane response as shown in Fig. 14a, b, one can conclude that the system is overdamped for *Gekko* and underdamped for *Varanus*. The value of the damping in the former would be $>\omega_*/4$ and $<\omega_*/4$ in the latter.

Given an initial guess, we can calculate the values of $\Re\{\Lambda_{\text{tot}}\}$ and $\Im\{\Lambda_{\text{tot}}\}$ at these values of f_0 and α from Eqs. (96) and (97). The value of the Jacobian can similarly be calculated by plugging these values into Eqs. (101)–(104) along with the values of $\widetilde{K}_{\text{mn}}$ given in Table 3. Thereafter one can iteratively use the Newton–Raphson method (98) until a suitable convergence is reached.

The simulation was performed for $N_{\text{modes}} = 1, 2, 5, 10,$ 15, 20, and 25 modes. The results of the simulation are presented in Table 5. For both *Gekko* and *Varanus*, we see that with an increasing number of eigenmodes used, the values converge to the quantities defined in Table 2. The slower convergence and apparent oscillation in α for *Gekko* is due to the higher value of its damping, which causes a greater difference between f_* and f_0. However, we must be careful while choosing initial guesses for *Varanus* as its lower damping results in a larger number of extrema and roots, and a simulation might converge to a point corresponding to a higher eigenmode. In practice, five modes are more than sufficient for good convergence in both f_0 and α. As a side remark, we need to emphasize that the numbers behind the decimal point in Tables 4 and 5 are experimentally irrelevant but are there just to demonstrate the accuracy of the numerical procedure.

Table 5 Simulation results

N_{modes}	*Gekko*		*Varanus*	
	f_0 (Hz)	α (s^{-1})	f_0 (Hz)	α (s^{-1})
1	1097.78	2490.72	402.664	347.637
2	1074.34	2589.08	401.074	349.942
5	1058.12	2611.35	400.333	350.108
10	1052.66	2612.18	400.108	350.046
15	1051.89	2612.09	400.077	350.034
20	1051.02	2611.87	400.041	350.02
25	1050.92	2611.84	400.037	350.018
Exact	1050	2611.45	400	350

In summary, and focusing on f_0, as a rule of thumb one can take the location of the minimum of the contralateral amplitude on the tonotopic axis or, equivalently, the maximum of the iLD or, if one likes f_* as the fundamental frequency f_0, the error being at most 5 %. Determining the damping coefficient α is a bit more work. The procedure outlined in Eqs. (96)–(107) gives us a systematic method to approximate α from the membrane vibrations for an arbitrary number of modes. In Table 5, we see that assuming f_* to be the fundamental frequency, which is equivalent to assuming $f_0 = f_*$, gives us a value of α with an error of at most 5 %. Taking into account the second mode further reduces the error to within 1 %. In fact, for the case of a single mode, the expression for α can be written down explicitly by substituting $\omega_0 = \omega_{11} = \omega_*$ in (97) giving us

$$\frac{K_{11}}{2\alpha\omega_*} = \frac{\eta V_{\text{cav}}}{\rho c L \omega_*}. \tag{108}$$

$$\Rightarrow \alpha = \frac{\rho c L K_{11}}{2\eta V_{\text{cav}}} = \frac{8\rho c L}{\pi^2 V_{\text{cav}}} \frac{\mathscr{S}_{\text{tymp}}}{\rho_M d_M} \frac{\widetilde{K}_{11}}{\eta}. \tag{109}$$

We thus have (109) as an expression for the membrane damping coefficient α given only the geometrical and material parameters (thickness and density) of the membrane and cavity and η—the iLD measurement at a given frequency.

References

Asmar NH (2005) Partial differential equations with Fourier series and boundary value problems. Pearson Education, New York

Autrum H (1942) Schallempfang bei Tier und Mensch. Naturwissenschaften 30:69–85

Christensen-Dalsgaard J (2005) Directional hearing in non-mammalian tetrapods. In: Popper AN, Fay RR (eds) Sound source localization. Springer handbook in auditory research. Springer, New York, pp 67–123

Christensen-Dalsgaard J, Manley GA (2005) Evolution of a sensory novelty: tympanic ears and the associated neural processing. J Exp Biol 208:1209–1217

Christensen-Dalsgaard J, Manley GA (2008) Acoustical coupling of lizard eardrums. J. Assoc Res Otolaryngol 9:407–416

Christensen-Dalsgaard J, Carr CE (2009) Evolution of a sensory novelty: tympanic ears and the associated neural processing. Brain Res Bull 75:365–370

Christensen-Dalsgaard J, Tang Y, Carr CE (2011) Binaural processing by the Gecko auditory periphery. J. Neurophysiol 105:1992–2004

Copson ET (1973) Introduction to the theory of functions of a complex variable. Clarendon Press, Oxford

Fletcher NH (1992) Acoustic systems in biology. Oxford University Press, Oxford

Heider D, Vedurmudi AP, van Hemmen JL (2016) Acoustic boundary condition dynamics and internally coupled ears (in preparation). This paper gives a mathematical justification of the perturbative approach presented here. See also: van Hemmen JL (2016) Acoustic boundary-condition dynamics and internally coupled ears. SIAM News 49/8:1–3

Jørgensen MB (1993) Vibrational patterns of the anuran eardrum. In: Elsner N, Heisenberg M (eds) Gene–brain–behaviour. Proceedings of the 21st Göttingen neurobiology conference. Georg Thieme Verlag, Stuttgart, p 231

Jørgensen MB, Kanneworff M (1998) Middle ear transmission in the grass frog Rana temporaria. J Comp Physiol A 182:59–64

Jørgensen MB, Schmitz B, Christensen-Dalsgaard J (1991) Biophysics of directional hearing in the frog Eleutherodactylus coqui. J Comp Physiol A 168:223–232

Koeppl C, Carr CE (2008) Maps of interaural time difference in the chicken's brainstem nucleus laminaris. Biol Cybern 98:541–559

Manley GA (1972a) The middle ear of the *Tokay gecko*. J Comp Physiol 81:239–250

Manley GA (1972b) Frequency response of the middle ear of Geckos. J Comp Physiol 81:251–258

Manley GA (2000) Cochlear mechanisms from a phylogenetic viewpoint. Proc Natl Acad Sci USA 97:11736–11743

Michelsen A, Larsen ON (2008) Pressure difference receiving ears. Bioinspir Biomim 3:011001

Pozrikidis C (2009) Fluid dynamics: theory, computation, and numerical simulation. Springer, New York

Rajalingham C, Bhat RB (1998) Vibration of circular membrane backed by cylindrical cavity. Int J Mech Sci 40:723–734

Rschevkin SN (1963) A course of lectures on the theory of sound. Pergamon, Oxford, p 111

Schnupp JW, Carr CE (2009) On hearing with more than one ear: lessons from evolution. Nat Neurosci 12:692–697

Stoer J, Bulirsch R (2002) Introduction to numerical analysis, 3rd edn. Springer, New York

Szpir MR, Sento S, Ryugo DK (1990) Central projections of cochlear nerve fibers in the alligator lizard. J Comp Neurol 295:530–547

Temkin S (1981) Elements of acoustics. Wiley, New York

van Hemmen JL, Christensen-Dalsgaard J, Carr CE, Narins P (2016) Animals & ICE: meaning, origin, and diversity. Biol Cybern 110(4–5). doi:10.1007/s00422-016-0702-x

Vedurmudi AP, Goulet J, Christensen-Dalsgaard J, Young BA, Williams R, van Hemmen JL (2016) How internally coupled ears generate temporal and amplitude cues for sound localization. Phys Rev Lett 116:028101

Vossen C (2010) Auditory information processing in systems with internally coupled ears. Doctoral dissertation, Technische Universität München

Vossen C, Christensen-Dalsgaard J, van Hemmen JL (2010) An analytical model of internally coupled ears. J Acoust Soc Am 128:909–918

Young BA, Vedurmudi AP, van Hemmen JL (2016) Auditory balance (in preparation)